JGR Solid Earth

RESEARCH ARTICLE
10.1029/2023JB027565

Inverting Geodetic Strain Rates for Slip Deficit Rate in Complex Deforming Zones: An Application to the New Zealand Plate Boundary

Kaj M. Johnson[1], Laura M. Wallace[2,3,4], Jeremy Maurer[5], Ian Hamling[6], Charles Williams[6], Chris Rollins[6], Matt Gerstenberger[6], and Russ Van Dissen[6]

[1]Department of Earth and Atmospheric Sciences, Indiana University, Bloomington, IN, USA, [2]University of Texas Institute for Geophysics, Austin, TX, USA, [3]GEOMAR Helmholtz Centre for Ocean Research Kiel, Kiel, Germany, [4]Institute of Geosciences, Christian-Albrechts-Universität zu Kiel, Kiel, Germany, [5]Departments of Geosciences and Geological & Petroleum Engineering, University of Missouri Science and Technology, Rolla, MO, USA, [6]GNS Science, Lower Hutt, New Zealand

Key Points:

- We develop a method to invert geodetically derived strain rates for slip deficit rates on faults
- We find small but systematic differences between slip deficit rates and geologic slip rates
- About 70%–80% of the surface strain can be attributed to elastic strain due to coupling on faults

Supporting Information:

Supporting Information may be found in the online version of this article.

Correspondence to:

K. M. Johnson,
kajjohns@indiana.edu

Citation:

Johnson, K. M., Wallace, L. M., Maurer, J., Hamling, I., Williams, C., Rollins, C., et al. (2024). Inverting geodetic strain rates for slip deficit rate in complex deforming zones: An application to the New Zealand plate boundary. *Journal of Geophysical Research: Solid Earth*, *129*, e2023JB027565. https://doi.org/10.1029/2023JB027565

Received 27 JULY 2023
Accepted 24 FEB 2024

Author Contributions:

Conceptualization: Kaj M. Johnson, Laura M. Wallace
Data curation: Jeremy Maurer, Ian Hamling, Charles Williams, Russ Van Dissen
Formal analysis: Kaj M. Johnson, Laura M. Wallace, Jeremy Maurer, Ian Hamling, Charles Williams, Chris Rollins
Funding acquisition: Matt Gerstenberger
Methodology: Kaj M. Johnson
Project administration: Matt Gerstenberger
Supervision: Matt Gerstenberger, Russ Van Dissen
Writing – original draft: Kaj M. Johnson, Laura M. Wallace

Abstract

The potential for future earthquakes on faults is often inferred from inversions of geodetically derived surface velocities for locking on faults using kinematic models such as block models. This can be challenging in complex deforming zones with many closely spaced faults or where deformation is not readily described with block motions. Furthermore, surface strain rates are more directly related to coupling on faults than surface velocities. We present a methodology for estimating slip deficit rate directly from strain rate and apply it to New Zealand for the purpose of incorporating geodetic data in the 2022 revision of the New Zealand National Seismic Hazard Model. The strain rate inversions imply slightly higher slip deficit rates than the preferred geologic slip rates on sections of the major strike-slip systems including the Alpine Fault, the Marlborough Fault System and the northern part of the North Island Fault System. Slip deficit rates are significantly lower than even the lowest geologic estimates on some strike-slip faults in the southern North Island Fault System near Wellington. Over the entire plate boundary, geodetic slip deficit rates are systematically higher than geologic slip rates for faults slipping less than one mm/yr but lower on average for faults with slip rates between about 5 and 25 mm/yr. We show that 70%–80% of the total strain rate field can be attributed to elastic strain due to fault coupling. The remaining 20%–30% shows systematic spatial patterns of strain rate style that is often consistent with local geologic style of faulting.

Plain Language Summary

The potential for future earthquakes on faults is often inferred from velocities of the ground surface derived from satellite geodesy, but this approach can be challenging in complex deforming zones with many closely spaced faults. We present a new methodology for estimating the rate at which energy is accumulating on faults using measurements of surface strain rates. The method is applied to New Zealand for the purpose of incorporating geodetic data in the 2022 revision of the New Zealand National Seismic Hazard Model. We show that 70%–80% of the total deformation field can be attributed to energy accumulation on known active faults while the source of the remaining 20%–30% remains unknown. Along some of the major faults in New Zealand we find some important differences in rates of energy accumulation from what is expected from geologic data. Estimated rates are significantly lower than even the lowest geologic estimates on some faults in the fault system near highly-populated Wellington.

1. Introduction

Since the early 1990's, our understanding of plate boundary zone crustal deformation has been revolutionized by advances in satellite-based geodetic techniques using Global Navigation Satellite Systems (GNSS) and Interferometric Synthetic Aperture Radar (InSAR). Such methods allow us to directly track the movement of the ground in real time and quantify the distribution and rate of tectonic strain accumulation within plate boundary zones. Typically, geodetic data are used to infer the distribution of present-day deformation across complex plate boundary zones such as New Zealand (Figure 1) by computing strain rates (e.g., Beavan & Haines, 2001; Haines & Wallace, 2020; Kreemer et al., 2000) or estimating fault slip rates using kinematic deformation models (e.g., Bird, 2009a; McCaffrey, 2005; Meade & Hager, 2005; Wallace et al., 2004; Zeng & Shen, 2014).

Writing – review & editing: Jeremy Maurer, Ian Hamling, Charles Williams, Chris Rollins, Russ Van Dissen

The fundamental assumption behind many models of contemporary geodetic data is that most of the present-day strain rate field is recoverable elastic deformation accumulating in the Earth's crust during the time between large earthquakes (the interseismic period) (e.g., Savage, 1983; McCaffrey, 2005; Mazzotti et al., 2000; Wallace et al., 2004). A number of different kinematic modeling techniques have been developed to infer fault slip rates from geodetic data, and a growing application of these geodetic techniques is to provide inputs for probabilistic seismic hazard analysis. For example, the Unified California Earthquake Rupture Forecast Version 3 (UCERF3; (Field et al., 2014)), the 2014 update to the US National Seismic Hazard Model (2014 US NSHM; Petersen et al. (2014)), and more recently the 2023 update the US NSHM (2023 US NSHM; Pollitz et al. (2022)), all used kinematic models of geodetic data to infer fault slip rates as inputs to the hazard model calculations. The UCERF3 and US NSHM projects utilized geodetic data in deformation models by undertaking joint modeling of geologic fault slip rates and the interseismic GPS-derived velocity field to estimate fault slip rates using several different approaches, including: Elastic block models (e.g., McCaffrey, 2005; Johnson & Fukuda, 2010; Hammond et al., 2011; Evans et al., 2015), deep-slipping dislocation models (Zeng & Shen, 2014, 2016), NeoKinema (Bird, 2009b), and viscoelastic fault models (Pollitz et al., 2008).

Rather than model individual faults, other studies have characterized the distribution of present-day deformation across plate boundary zones by computing surface strain rates from geodetic data (e.g., Beavan & Haines, 2001; Haines & Wallace, 2020; Weiss et al., 2020; Kreemer & Young, 2022). Sometimes the surface strain rates are used to compute the spatial distribution of moment accumulation rate in the crust (e.g., Ward, 1998; Savage & Simpson, 1997), however it is not straightforward with such approaches to associate surface strain with any particular fault at depth. Several studies have shown that estimation of the long-term spatial distribution of earthquakes for Probabilistic Seismic Hazard Analysis is improved with the use of geodetically derived strain rate data (Bird et al., 2015; Kreemer et al., 2002; Mazzotti et al., 2011; Rastin et al., 2022; Rhoades et al., 2017).

The purpose of this study is to present a method for inverting surface strain rates directly for slip deficit rates on faults in complex zones where it is difficult to implement traditional kinematic deformation models. The method is developed specifically for the purpose of incorporating geodetically based fault slip deficit rates in the 2022 update to the New Zealand National Seismic Hazard Model (NZ NSHM 2022). However, the method described in this paper differs from previously used methodologies for incorporating geodetic data into seismic hazard models. For this project we use an approach which inverts the strain rate field (rather than the velocity field) for backslip (or slip deficit rate) on crustal faults in the New Zealand Community Fault Model (NZ NSHM 2022 fault model). The need to estimate a geodetic slip rate for all 703 faults considered in NZ NSHM 2022 (Figure 1) makes the use of elastic block models challenging, requiring a complex model with hundreds of independent tectonic blocks bounded by faults that would require heavy regularization (e.g., Evans et al., 2015; Evans, 2022). Deep-slipping dislocation models (e.g., Beavan et al., 1999; Zeng & Shen, 2016) provide a means to determine long-term fault slip rates below the portion of the fault that is locked, and the derived strain rates are mathematically equivalent to backslip models. However, fitting the rapid tectonic rotation of the eastern North Island observed in the velocity field (Wallace et al., 2004) would be difficult, if not impossible to fit with such an approach. Inverting strain rates for slip deficit rates avoids the need to utilize elastic block models to fit tectonic block rotations inherent to the New Zealand GNSS velocity field because block rotations are rigid-body motions that produce zero strain rate. Further, a key advantage to the approach is that it immediately determines the slip deficit rate (or moment accumulation rate), which is directly relevant to the rate of elastic strain accumulation, much of which we assume will be relieved in future earthquakes.

For this study, we use four strain rate maps for New Zealand that were prepared for the NZ NSHM 2022 (Maurer et al., 2023). The strain rate maps were constructed using New Zealand's interseismic campaign GPS-derived velocity field spanning 1995–2013 (Beavan et al., 2016).

2. Deformation Across the New Zealand Plate Boundary

New Zealand is situated in the deforming zone between the Pacific and Australian Plates, where ongoing relative plate motion is accommodated across a complex array of active faults (Figure 1). The principal kinematics of present-day deformation within the plate boundary are illustrated with NZ NSHM 2022 geologic deformation model slip rates and rake angles in Figure 1. In the South Island, the Alpine Fault marks the plate boundary and accommodates as much as 30 mm/yr of right-lateral motion. The Alpine Fault transitions northward to the Marlborough Fault System (MFS) in the northeastern South Island which is a zone of four sub-parallel faults with

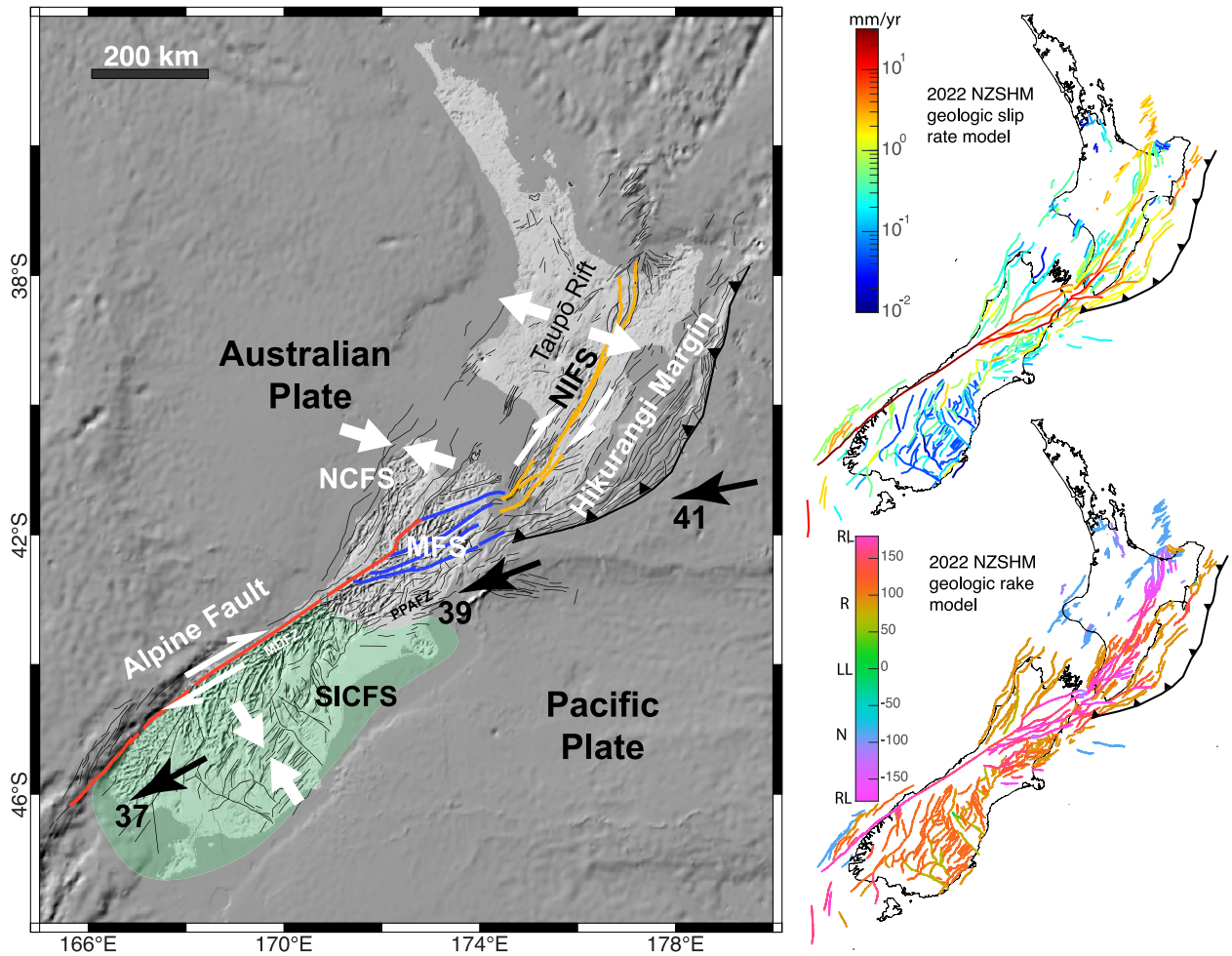

Figure 1. Active tectonic setting of the New Zealand plate boundary showing major tectonic fault systems. Slip rates and rake are from the 2022 New Zealand National Seismic Hazard Model (NZ NSHM). Black arrows show convergence rate (mm/yr) of Pacific Plate relative to Australian Plate. White arrows show general sense of deformation across and within various tectonic regions. Thin black lines show active fault traces from the NZ NSHM 2022 fault model. MFS = Marlborough Fault System, NIFS = North Island Fault System. SICFS = South Island Contractional Fault System, NCFS = Nelson Contractional Fault System. PPAFZ = Porters Pass/Amberley Fault Zone. MDFZ = Main Divide Fault Zone.

largely right-lateral strike-slip motion (Holt & Haines, 1995; Van Dissen & Yeats, 1991). The Porter's Pass Fault Zone in northern Canterbury accommodates several mm/yr of oblique transpression (Pettinga et al., 2001; Wallace et al., 2007) southeast of the Marlborough Fault System. Lower rates of more distributed contraction occur on faults in the northwestern South Island, and also east of the southern Alps and in the Otago region, with fault slip rates generally less than 1 mm/yr. North Island tectonics is dominated by subduction of the Pacific Plate at the Hikurangi subduction zone, and slip partitioning is accommodated by the North Island Fault System (NIFS) which carries 5–10 mm/yr of the right lateral, strike-slip component of the oblique convergence between the Pacific and Australian Plate Beanland and Haines (1998). Rotation of the eastern North Island produces intra-arc extension in the Taupo Volcanic Zone of the central North Island.

An aggregate representation of the four geodetically derived strain rate models for the NZ NSHM 2022 (Maurer et al., 2023) is illustrated in Figure 2. The strain rate models were derived using a diverse range of approaches in order to explore and quantify the epistemic uncertainties introduced by calculation of strain rates from GNSS velocity fields. The four methods include the VDoHS method (Haines et al., 2015; Haines & Wallace, 2020), a method based on calculation of body force elastic Green's functions (Johnson et al., 2022), VELMAP (Wang & Wright, 2012; Weiss et al., 2020),and a method based on geostatistics (Maurer & Materna, 2023). The aggregate in Figure 2 is computed by averaging thousands of realizations of the four strain rate models, where each realization is drawn from the formal distributions of the estimated strain rate fields. Since the purpose of this work is

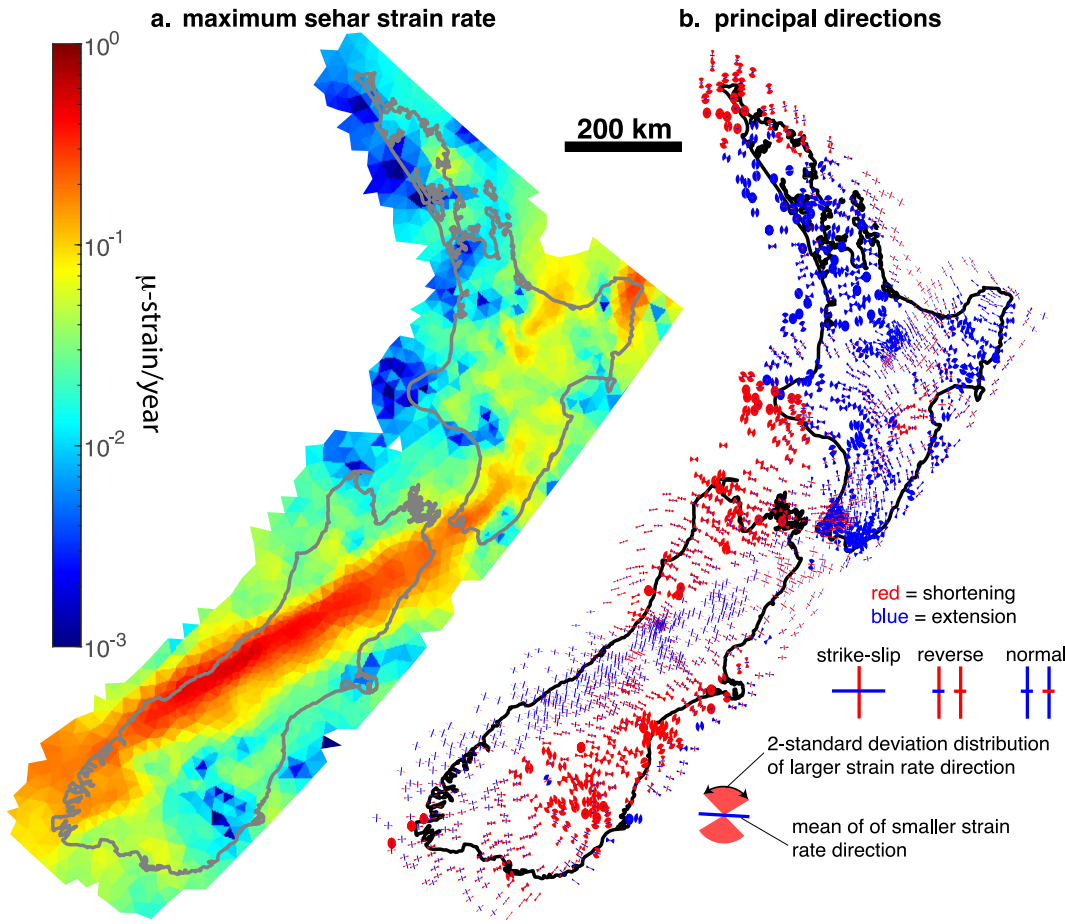

Figure 2. Aggregate of four geodetically derived strain rate models from Maurer et al. (2023). (a) Mean maximum shear strain rate with log color scale (maximum shear in terms of principal strain rates, $(\varepsilon_1 - \varepsilon_2)/2$). (b) Principal directions. Larger of the two horizontal principal strain rates shown with wedges providing the two standard deviation range. The smaller of the two principal directions is shown with a line. Red is shortening and blue is extension. Interpretation of principal strain rate directions in terms of style of faulting is illustrated.

to derive slip deficit rates for upper crustal faults for the NZ NSHM 2022, deformation due to coupling on the Hikurangi subduction interface was subtracted from the geodetic velocity field that was used to compute the four NZ NSHM 2022 strain rate maps (Johnson et al., 2022). The coupling model used is an update to Wallace et al. (2012). The most prominent feature of the maximum shear strain rate field is the belt of high shear strain rates nearing one μ-strain/yr along the Alpine fault system through the South Island, continuing through the Marlborough Fault System and the southern part of the North Island Fault System, consistent with previously published strain rate models (Beavan & Haines, 2001; Haines & Wallace, 2020). The size of the uncertainty wedges in Figure 2b indicate that principal strain rate directions can be resolved in most regions of New Zealand with the exception of the lowest strain rate regions in part of the Otago and Northland regions.

As discussed by Maurer et al. (2023), the spatial distribution of the magnitudes and style of geodetically derived strain rate are qualitatively similar to the geologic model slip rates and rakes (Figure 1). That is expected, because a large portion of interseismic strain rate is thought to be attributed to elastic distortion of the crust due to interseismic coupling on faults. However, as noted previously, studies of the western United States suggest that only about 70% of the present-day strain rates can be associated with fault slip. In this study, we examine how much of the present-day strain rate field in New Zealand can be attributed to interseismic coupling on active faults. We do so by directly inverting the four strain rate maps for slip deficit rate, which is the long term fault slip rate minus the interseismic creep rate, or the rate at which slip available for future earthquakes is accumulating over time. The inversion scheme is described in the next section.

3. Slip Deficit Inversion Method

As is assumed in traditional elastic block models of velocity fields (e.g., Meade & Hager, 2005; McCaffrey, 2005), we assume that strain rates in the crust are generated solely by slip deficit rates on faults. That is, we assume that long-term fault slip and associated block motions between faults do not generate strain in the crust. This idea is can be originally attributed to the work of Savage and Burford (1970) and Savage (1983). Elastic block models typically assume long-term rigid body motions across faults and interseismic elastic deformation due to coupling on faults. Interseismic strain is generated with backslip on faults which has the effect of canceling or reducing the long-term slip rate generated by rigid body motions. Because our method utilizes surface strain rates rather than velocities, we do not need to estimate block motions or long-term faults slip rates and we only solve for backslip rates (equivalently, slip deficit rates) on faults, as described below. In this section, we provide a description of the methodology for inverting strain rates for slip deficit rates on faults. We discuss the construction of slip deficit Green's functions, the incorporation of geologic slip rate constraints as prior information, and the inversion scheme for constructing posterior probability distributions of the spatial distribution slip deficit rate in New Zealand.

3.1. Construction of Slip Deficit Green's Functions

To solve for the spatial distribution of slip deficit rate on faults, we will utilize the solution for uniform slip on a rectangular dislocation in an elastic half space (Okada, 1992) which provides surface displacements and gradients in displacement (strain). We represent the faults in New Zealand with a series of planar fault segments that are discretized into rectangular patches as illustrated in Figure 4. The nominal patch length along strike is 10 km and varies from 5 to 15 km, and the nominal down-dip width is 8 km and varies from 4 to 12 km. To construct this 3D fault model, we first approximate the surface traces of faults in the New Zealand NSHM 2022 fault model (Seebeck et al., 2023) with 10-km long piece-wise-continuous fault segments to smooth out shorter wavelength variations in fault strike and simplify some complex fault intersections. We adopt the preferred dip and rake from the fault model for each model segment. The planar fault segments are extended at constant dip from the surface to the D90 depth (depth of 90% of seismicity) in the NZ NSHM 2022 fault model.

One challenge with modeling strain rates with uniform slip dislocations solutions is that the strain rate field near the fault is highly sensitive to the discretization of slip rate gradients because strain rate is singular at dislocation edges. The implications of using uniform slip dislocations for modeling strain rate are illustrated in Figure 3 which shows the surface maximum shear strain rate for a vertical strike-slip fault in an elastic halfspace. The slip deficit rate distribution is uniform over 5 km long patches (slip deficit extends to 15 km depth) at the rates shown in Figure 3a. Figure 3b shows the resulting strain rates. Clearly, the imposed discontinuities in slip deficit rate introduce distinctive strain rate lobes emanating from the discontinuities. To avoid these lobes, we impose continuous, linear slip gradients on faults that maintain the average slip deficit rate over segments. The surface maximum shear strain rate pattern resulting from the linear slip deficit rate distribution is shown in Figure 3c. To compute the strain rate distribution, we subdivide the uniform slip patches into many smaller patches of length 0.5 km (15 km deep) and impose the slip rates shown in Figure 3a at the larger segment endpoints and impose a linear gradient between. The result of the linear tapering is a smoother surface strain rate field without the lobes of high strain rates.

Strain rate singularities also arise because of discontinuities in geometry, for example, sharp bends in the fault surface. Figure 3d illustrates a geometry similar to Figures 3a–3c, but with a kink due to a 20-degree sudden change in strike at point (0,0). The same linearly tapered slip distribution as in Figure 3c is imposed. Here the strain rate concentration near (0,0) is due to the kink in the fault. While such strain rate concentrations are not entirely unexpected in the crust, strain rate concentrations associated with complex, non-planar fault geometry depend on detailed knowledge of the fault geometry that we do not have access to and geodetic observations that are too sparse to resolve such features. To avoid the problem of fitting smooth observed strain rate fields with a model that contains strain rate artifacts due to arbitrary representations of faults as rectilinear segments, we compute strain rates at the centroids of triangles in a fault-based triangular mesh as illustrated in Figure 3d. The mesh is designed so that fault segment endpoints occur as nodes and fault traces occur as sides of triangles. This spacing of compute nodes minimizes the influence of singularities at fault endpoints and kinks on strain rate calculations. The mesh is constructed using the program MESH2D (Engwirda, 2014) which is an unstructured meshing algorithm based on Delaunay-refinement and hill-climbing mesh optimization.

Figure 3e shows the actual fault-based mesh we have adopted for New Zealand based on the surface trace approximations of the New Zealand NSHM 2022 fault model (Figure 1) (Seebeck et al., 2023). The maximum edge length of triangles is 15 km along faults and 100 km at the edge of the model domain.

3.2. Geologic Constraints

Geologic constraints on slip rates are adopted from the NZ NSHM 2022 Geologic Deformation Model (GDM). The GDM specifies preferred and upper and low limits for slip rake and slip rate for every fault segment. We fix the model rake to the preferred slip rake for each fault, and solve for the slip deficit rate in that fixed rake direction. Slip deficit rate is therefore constrained to be a positive number (non-negativity constraint). We incorporate the preferred, upper and lower geologic slip rates in the GDM by introducing truncated Gaussian prior distributions on slip deficit rate. The prior slip rate at any point along the fault is a truncated Gaussian distribution centered on the preferred geologic rate with 1-standard deviation equal to the geologic upper rate minus the lower rate. The distribution is truncated at zero at the low end and ten times the GDM high slip rate at the upper end. The rationale for this choice of prior is two-fold. The Gaussian shaped prior is convenient for use with linear error propagation, as described in detail in the following section. Second, the prior distribution favors the preferred geologic value, but conservatively permits slip rates above and below the upper and lower rates.

3.3. Inversion Scheme

We want to solve for the slip deficit rates on all rectangular slip patches from the three components of horizontal strain rate tensor for each of the four strain rate maps, subject to bound constraints. The objective is to solve for the full (correlated) posterior probability distribution of slip deficit rate on patches. This inversion is conducted in two steps. We first conduct a linear inversion for slip deficit rate without bound constraints and use linear error propagation to obtain the posterior distribution. In the second step, we numerically construct the posterior distribution with bound constraints by sampling using Monte Carlo methods.

First we set up the linear, unbounded inversion. Let $\mathbf{s}$ be a vector of slip deficit rates on all patches, let $\mathbf{d}_\epsilon$ be a vector of observed strain rates, and let $\mathbf{G}_\epsilon$ be the matrix of strain rate Greens functions. For this problem, we have 8,229 slip patches and 9,255 strain rate observations (3 components at 3,085 coordinate points). The basic observation equation is then

$$\mathbf{d}_\epsilon = \mathbf{G}_\epsilon \mathbf{s} + \epsilon \tag{1}$$

where ϵ is a vector of errors, assumed to be Gaussian. In this section we first introduce the geologic slip rate constraints in two equivalent ways: as a prior distribution or as data. Let $\mathbf{s}_p$ be a vector of preferred geologic slip rates on all patches, and let Σ_s be the diagonal covariance matrix with the slip deficit rate variances on the diagonal. We also construct diagonal covariance matrices for the strain rate data, Σ_ϵ. Covariances are ignored for this inversion because they are not provided by Maurer et al. (2023), but it would be valuable in future work to examine the consequences of ignoring covariances. If we treat the geologic constraints as data, we construct the following augmented observation equations

$$\begin{bmatrix} \Sigma_\epsilon^{-1/2}\mathbf{d}_\epsilon \\ \Sigma_s^{-1/2}\mathbf{s}_p \end{bmatrix} = \begin{bmatrix} \Sigma_\epsilon^{-1/2}\mathbf{G}_\epsilon \\ \Sigma_s^{-1/2}\mathbf{I} \end{bmatrix} \mathbf{s} + \epsilon \tag{2}$$

To simplify notation, we write the weighted observation vector, $\mathbf{d}_w$, on the left side of Equation 2 and weighted matrix, $\mathbf{G}_w$, on the right side of Equation 2 as

$$\mathbf{d}_w = \mathbf{G}_w \mathbf{s} + \epsilon \tag{3}$$

We require that the slip deficit rate vary smoothly on neighboring patches along fault segments by introducing the difference operator, $\mathbf{D}$, that computes differences in slip deficit rate in the along-strike and down-dip directions between patches. We then have the following system of equations to solve,

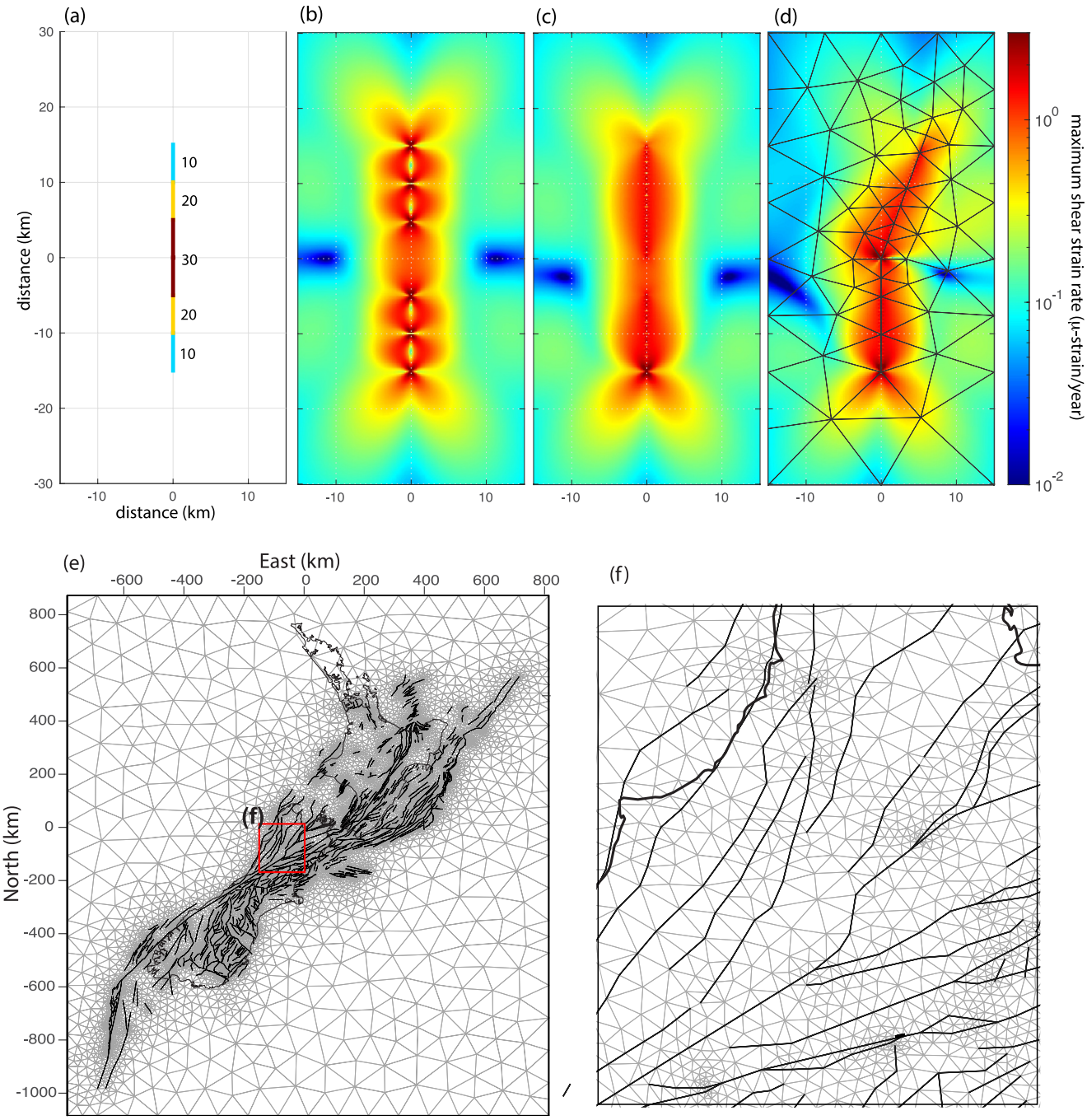

Figure 3. Illustration of strain rate calculations using linearly tapered slip distributions, as described in the text. (a) Input slip rate distribution (map view) on a vertical strike-slip fault extending from the surface to 15 km depth. (b) Computed maximum shear strain rate at the surface for non-tapered slip distribution (uniform slip rate over sections as illustrated in left side panel). (c) Maximum shear strain rates for linearly-tapered slip distribution. (d) Illustration of mesh construction used to minimize the influence of strain rate singularities due to terminations and kinks in faults. (e) Mesh used for computing strain rate Greens functions. Mesh size is controlled by fault trace geometry. Strains are computed at the center of each triangular element for unit slip on each rectangular fault patch shown in Figure 4b. (f) Enlargement of area shown in (e).

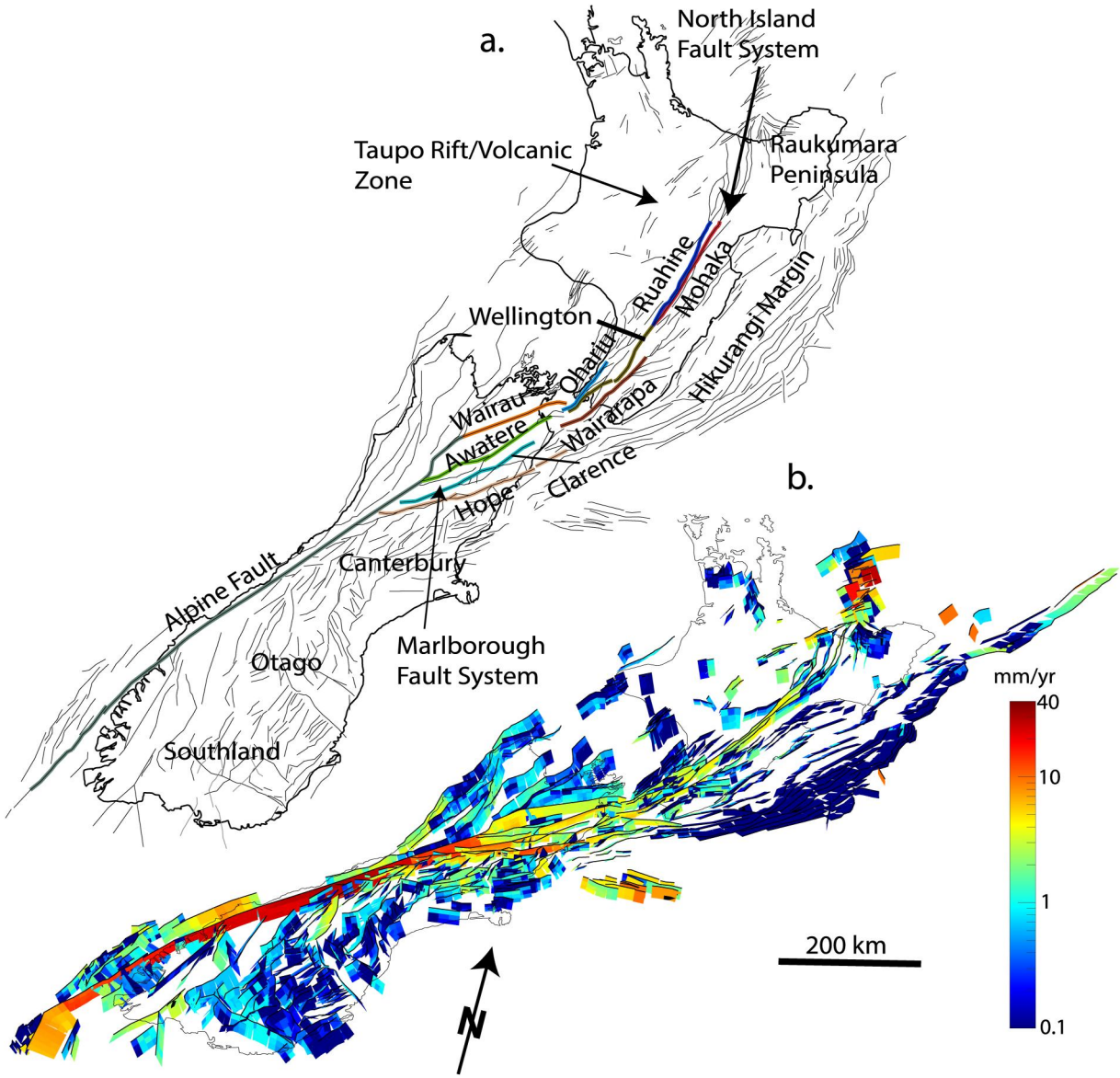

Figure 4. (a) Location of geographic and geologic features referred to in the discussion of results. (b) 3D perspective view of median slip deficit rates for "No Geologic Prior" inversion. This is the median of the four best-fitting inversions without geologic slip rate priors (one inversion for each strain rate map). Color shows slip deficit rate in mm/yr on logarithmic color scale.

$$\begin{bmatrix} \mathbf{d}_w \\ \mathbf{0} \end{bmatrix} = \begin{bmatrix} \mathbf{G}_w \\ \alpha^{-2}\mathbf{D} \end{bmatrix} \mathbf{s} + \epsilon \tag{4}$$

where the smoothing parameter, α, determines the relative weight placed on fitting the data versus maintaining smoothness in slip deficit rate. Equation 4 can be solved using standard least squares formula. Equivalently, we can introduce the generalized inverse,

$$\mathbf{G}^{\#} = \left[\mathbf{G}_w^T \mathbf{G}_w + \alpha^{-2}\mathbf{D}^T\mathbf{D}\right]^{-1} \mathbf{G}_w^T \tag{5}$$

and obtain the least squares solution as,

$$\mathbf{s}_\alpha = \mathbf{G}^\sharp \mathbf{d}_w \tag{6}$$

which is the best-fitting slip deficit rate distribution for a given smoothing parameter, α. The covariance matrix for slip deficit rate is then,

$$\mathbf{\Sigma}_\alpha = \mathbf{G}^\sharp \begin{bmatrix} \Sigma_\varepsilon & \mathbf{0} \\ \mathbf{0} & \Sigma_s \end{bmatrix} \left(\mathbf{G}^\sharp\right)^T \tag{7}$$

In this study, the value for smoothing parameter, α, is selected using a trade-off curve. More objective methods for selecting smoothing have been explored in the literature including cross-validation (e.g., Matthews & Segall, 1993), Bayesian methods (e.g., Fukuda & Johnson, 2008; Fukahata & Wright, 2008; Minson et al., 2013), and physical constraints (e.g., Herman & Govers, 2020; Jiang et al., 2022).

Now to incorporate the bound constraints on slip deficit rate, we switch notation to express the problem in terms of probability density functions. Bayes' Theorem states

$$p(\mathbf{s}|\mathbf{d}) \propto p(\mathbf{d}|\mathbf{s})p(\mathbf{s}) \tag{8}$$

where $p(\mathbf{s}|\mathbf{d})$ is probability density of slip deficit rate given data, $\mathbf{d}$, $p(\mathbf{d}|\mathbf{s})$ is Likelihood, and $p(\mathbf{s})$ is the prior probability distribution of slip deficit rate (e.g., Mosegaard & Tarantola, 1995). If we continue to view the geologic constraints as data then the likelihood is

$$p(\mathbf{d}|\mathbf{s}) \propto \exp\left\{-0.5(\mathbf{d}_w - \mathbf{G}_w\mathbf{s})^T(\mathbf{d}_w - \mathbf{G}_w\mathbf{s})\right\} \tag{9}$$

with the prior distribution, $p(\mathbf{s})$, taken as box-car distributions (uniform distribution between upper and lower bounds, zero outside). Because the relationship between data and slip deficit is linear, the Likelihood is a multivariate Gaussian distribution, and we can write the distribution using the least squares solution (Equations 6 and 7)

$$p(\mathbf{s}|\mathbf{d}) = p(\mathbf{d}|\mathbf{s}) \propto \exp\left\{-0.5(\mathbf{s} - \mathbf{s}_\alpha)^T\mathbf{\Sigma}_\alpha^{-1}(\mathbf{s} - \mathbf{s}_\alpha)\right\} \tag{10}$$

Equivalently, we can view the geologic constraints as a prior probability distribution on slip deficit rate, and formulate spatial smoothing as a prior distribution, and write the prior distribution as a product of distributions, $p(\mathbf{s}) = p(\mathbf{s}|\alpha)\mathrm{g}(\mathbf{s})b(\mathbf{s})$, where $\mathrm{g}(\mathbf{s})$ is a multivariate Gaussian distribution representing the geologic priors, $b(\mathbf{s})$ are box-car functions that truncate the Gaussian distributions, and $p(\mathbf{s}|\alpha)$ is

$$p(\mathbf{s}|\alpha) \propto \exp\left\{\frac{-1}{2\alpha^2}(\mathbf{Ds})^T(\mathbf{Ds})\right\} \tag{11}$$

Then we can write the posterior distribution on slip deficit rate given strain rate data as,

$$p(\mathbf{s}|\mathbf{d}_\varepsilon) \propto p(\mathbf{d}_\varepsilon|\mathbf{s})\, p(\mathbf{s}|\alpha)g(\mathbf{s})b(\mathbf{s}) \tag{12}$$

where the Likelihood in Equation 12 is

$$p(\mathbf{d}_\varepsilon|\mathbf{s}) \propto \exp\left\{-0.5(\mathbf{d}_\varepsilon - \mathbf{G}_\varepsilon\mathbf{s})^T\Sigma_\varepsilon^{-1}(\mathbf{d}_\varepsilon - \mathbf{G}_\varepsilon\mathbf{s})\right\} \tag{13}$$

The distribution $p(\mathbf{d}_\varepsilon|\mathbf{s})p(\mathbf{s}|\alpha)g(\mathbf{s})$ in Equation 12 is the same distribution as Equation 10, which is formulated using least squares and error propagation. Then we can write,

$$p(\mathbf{s}|\mathbf{d}_\varepsilon) \propto p(\mathbf{d}|\mathbf{s})b(\mathbf{s}) \tag{14}$$

Table 1
Variance Reduction for Sixteen Different Slip Deficit Rate Inversions

	Velmap	VDoHS	GeoStats	BodyForce
No Geologic Prior	71.7	75.5	67.8	79.0
Geologic Prior	70.2	72.9	55.1	76.9
Strict Bounds	57.9	65.0	54.7	66.9
Fixed	38.3	48.8	38.6	47.4

Note. Variance reduction defined as $\left[1 - \|r\|^2/\|d\|^2\right] x100\%$ where $\|r\|$ is the Euclidean length of the residual vector and $\|d\|$ is the Euclidean length of the data vector. All inversions impose non-negative bounds. The four different inversion types are described in the main text.

where $p(\mathbf{d}|\mathbf{s})$ is given by Equation 10. The distribution in Equation 14 must be obtained numerically because of the bounds expressed in $b(\mathbf{s})$ preclude a closed-form expression. Therefore, we sample Equation 14 using the Monte Carlo Metropolis-Hastings algorithm (e.g., Mosegaard & Tarantola, 1995), which is much more efficient than sampling Equation 12 because we have removed the need to compute many matrix-vector products.

4. Results

We conduct four different inversions for each of the four strain rate maps (summarized by the aggregate strain rates in Figure 2). All inversions assume smoothing parameter $\alpha = 1$ which was selected from a trade-off curve using the VDoHS strain rate map (see Figure S1 in Supporting Information S1). The results of the sixteen inversions are summarized in Table 1. The first inversion adopts a uniform prior on slip deficit rate (no preferred rate) with a lower bound of zero (to prevent backwards slip) and an upper bound equal to ten times the Geologic Deformation Model (GDM) high slip rate. This is called the "No Geologic Prior" inversion because geologic constraints are only used very loosely to bound slip deficit rates within an order of magnitude of the GDM rate. The second inversion assumes the truncated Gaussian prior distributions based on the geologic upper slip rates as described in Section 3.2, and is called the "Geologic Prior" inversion. For the sake of comparison, and to illustrate the influence of the GDM constraints on inversion results, we also conduct a "Strict Bounds" inversion where the slip deficit rates are forced to lie between the GDM low and high slip rates using uniform, bounded prior distributions. The final result, called "Fixed" is not an inversion at all; we fix the slip deficit rates to be exactly equal to the preferred geologic slip rates. The Variance reduction for each of these sixteen models is given in Table 1. Unsurprisingly, the "No Geologic Prior" inversions fit the data best, with variance reduction ranging from 68% to 79%. The Fixed model explains less than half the data, with variance reduction ranging from 38% to 49%.

Figure 4 illustrates the median slip deficit rate distribution for the "No Geologic Prior" inversions with a 3D perspective view of slip deficit rate on all of the rectangular slip patches. As expected, the highest slip deficit rates occur along the major strike-slip fault systems including the Alpine Fault, the Marlborough Fault System and the North Island Dextral Fault Belt. Slip deficit rates on offshore faults are not reliable (and highly uncertain) because of the lack of geodetic data offshore. Figure 5 illustrates how much of the observed strain rate field can be explained by slip deficit rate on faults in NZ NSHM 2022 fault model. The figure compares the mean maximum shear strain rate and dilatation of the four strain rate maps with the mean rates of the four "No Geologic Prior" inversions. The residual strain rates are computed by subtracting the mean model strain rates from the mean observed rates. As shown in Table 1, this inversion result explains about 70%–80% of the total strain rate field. The residual maximum shear strain rates and dilatation rate maps (Figure 5) show the 20%–30% of the total strain rate field that is not explained by slip deficit rates on faults. The uncertainties in maximum shear strain rate range from 0.01 to 0.05 micro-strain/yr and uncertainties in dilatation rate are of order 0.02 to 0.05 micro-strain/yr for the VDoHS, body force and VELMAP solutions (Maurer et al., 2023); the uncertainties are several times larger in the geostatistics solution. Residual maximum shear strain rates exceed these uncertainties in the Taupo Volcanic zone, at the southern edge and south of the Marlborough Fault system, and in the NW edges of the Otago and Southland regions (locations in Figure 4a). Residual dilation rates exceed uncertainties in a number of areas and the modeled dilatation pattern is considerably more heterogeneous spatially than in the strain rate maps. We see residual expansion (blue) along the SE coast of the North Island and in the Taupo Volcanic region. The residual dilatation pattern is more heterogeneous in the South Island. We discuss the nature of the residual strain rate field in more detail later in this paper. In the following figures, we describe the estimated slip deficit rates in more detail.

Figure 6a compares the depth-averaged slip deficit rates for each of the four "No Geologic Prior" inversions on a logarithmic color scale. The differences between models are typically at the level of a few mm/yr or less onshore. The offshore slip deficit rates vary significantly, but this occurs because the offshore slip deficit rates are not well constrained due to lack of offshore geodetic data. Figure 6b shows the difference between the mean depth-averaged slip deficit rates for each inversion and the Geologic Deformation Model preferred slip rate on each fault section. There are systematic differences between the geologic deformation model preferred rates and the inverted slip deficit rates at the level of >1 mm/yr. The geodesy based inversions infer higher slip rates on the

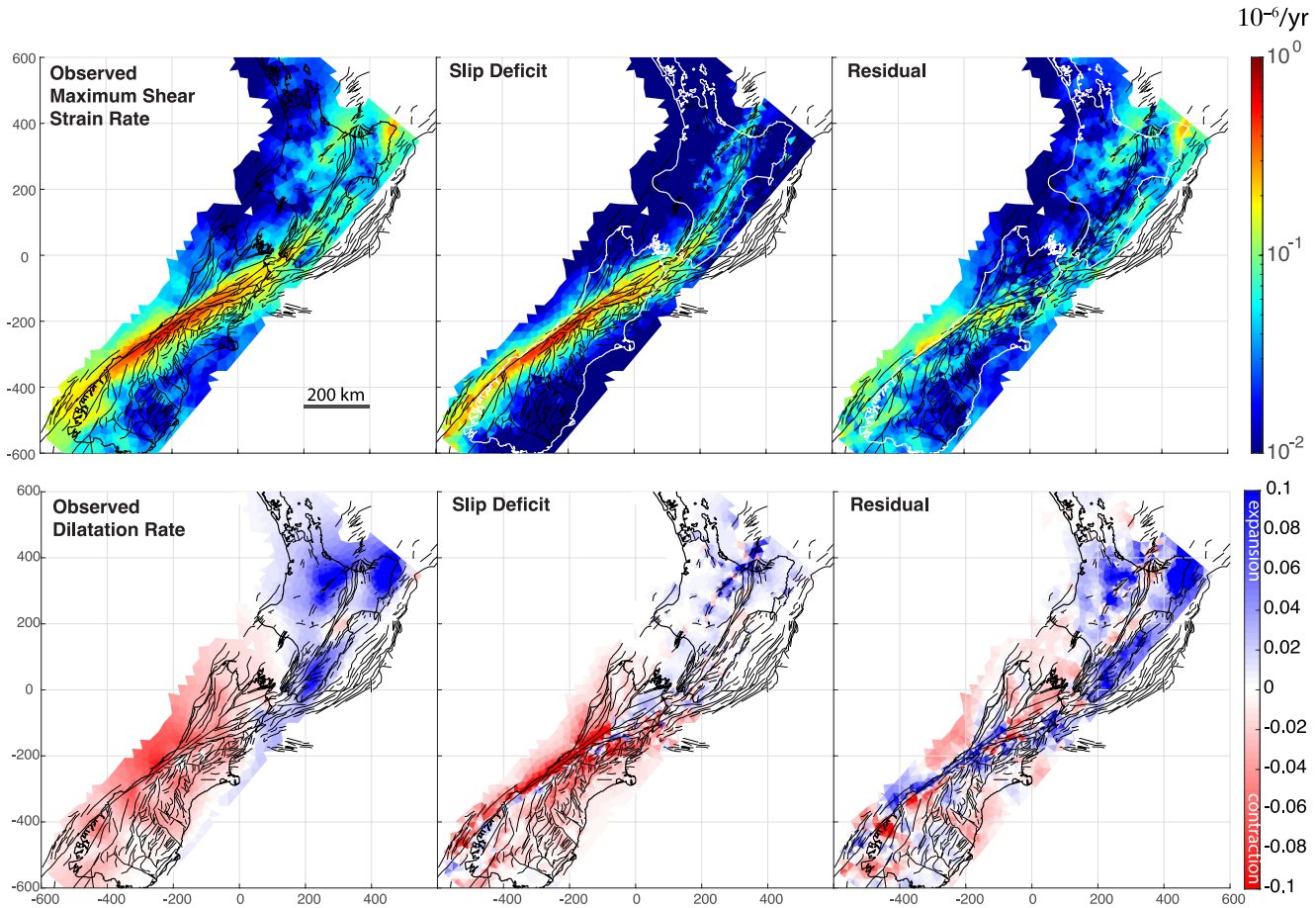

Figure 5. Comparison of observed and modeled strain rates ("No Geologic Prior" inversion) computed from the average of the four strain rate maps and the average of the means of the four strain rate inversions. Left side panels are observed maximum shear strain rates and dilatation rates. Middle panel shows modeled strain rates (strain rates due to slip deficit on faults). Right-side panel shows observed minus modeled (residual strain rates).

major strike-slip systems including the Alpine Fault, the Marlborough Fault System and the North Island Fault System. The geodesy-based inversions also infer systematically higher slip deficit rates SW of the Marlborough Fault System and scattered throughout the Otago region. The geodetic rates are systematically lower along the nearshore part of the Hikurangi margin.

Figure 7 compares the aggregate slip deficit rates by fault section with the preferred slip rate from the Geologic Deformation Model (GDM). Although there is overall good agreement between the geologic slip rates and the geodetic slip rates, it is interesting to note that the cluster of points trends along a line with slope less than one for both sets of inversions indicating a systemic mismatch. Specifically, for fault sections with GDM rates less than about 1 mm/yr, there is a tendency for the geodetic slip deficit rates to be higher than the GDM rates, while for sections with GDM rates above 1 mm/yr, the geodetic slip deficit rates tend to be lower. This result is discussed in more detail in the Discussion section.

Figure 8 summarizes along-fault, depth-averaged slip deficit rates for some of the higher slip rate faults in New Zealand for both the "No Geologic Prior" and "Geologic Prior" inversions. The inversion results for the four strain rate maps are aggregated into a single combined estimate by numerically summing an equal number of realizations of slip deficit rates from each strain rate map inversion. The aggregate mean is shown with solid lines and the aggregate 95% confidence intervals are shown with shaded regions. For comparison, the figure also shows the preferred, upper, and lower slip rates from the geologic slip rate model. The aggregate 95% confidence range of slip deficit rate is about 4 mm/yr for all these high-rate faults. As described in the model description section, slip deficit rates are smoothed across fault segments but discontinuities in slip deficit rate are allowed at intersections of fault segments, as seen for example, at ∼100 km distance along the Awatere Fault. In the "No

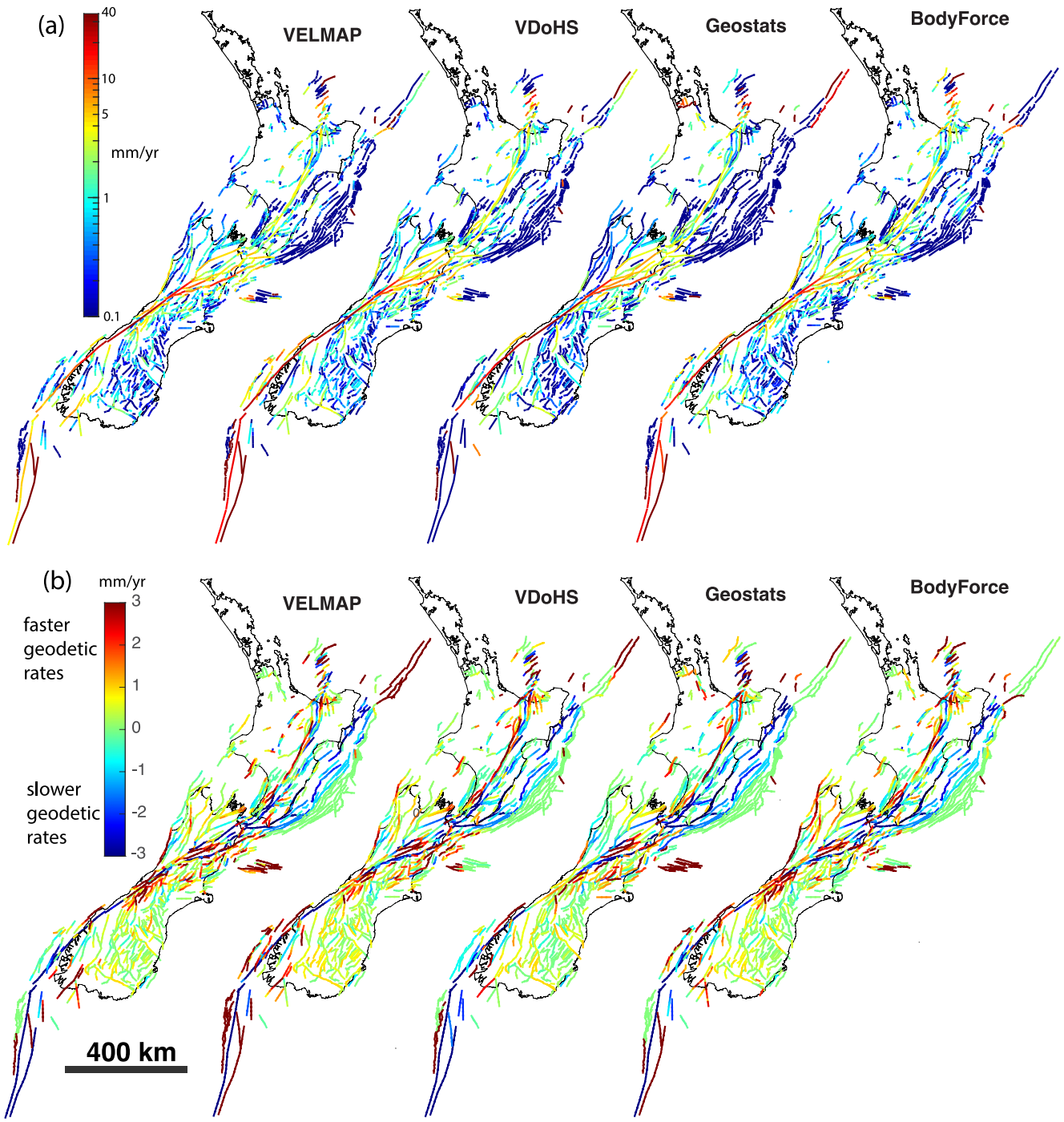

Figure 6. (a) Mean depth-averaged slip deficit rates for the four strain rate map inversions ("No Geologic Prior" inversion). Slip deficit rates shown along fault traces with logarithmic color scale. (b) Difference between mean depth-averaged slip deficit rates and preferred geologic rates for the four strain rate map inversions. Slip deficit rate differences (geodetic minus geologic) shown along fault traces with logarithmic color scale.

Geologic Prior" estimate, there are some significant deviations in model slip deficit rates from the geologic model (GDM). In particular, the geodetically derived slip deficit rates at the 95% confidence level, are lower than the geologic model slip rates along much of the Hope, Wairarapa and Wellington Faults, but higher along sections of the Clarence, Ohariu, and Ruahine Faults. The slip deficit rates on the Alpine Fault agree extremely well with the geologic estimates with the exception of the offshore southern end of the Alpine Fault, beginning at about 500 km distance along the profile in Figure 8, where rates are all systematically lower than the geologic model slip rates.

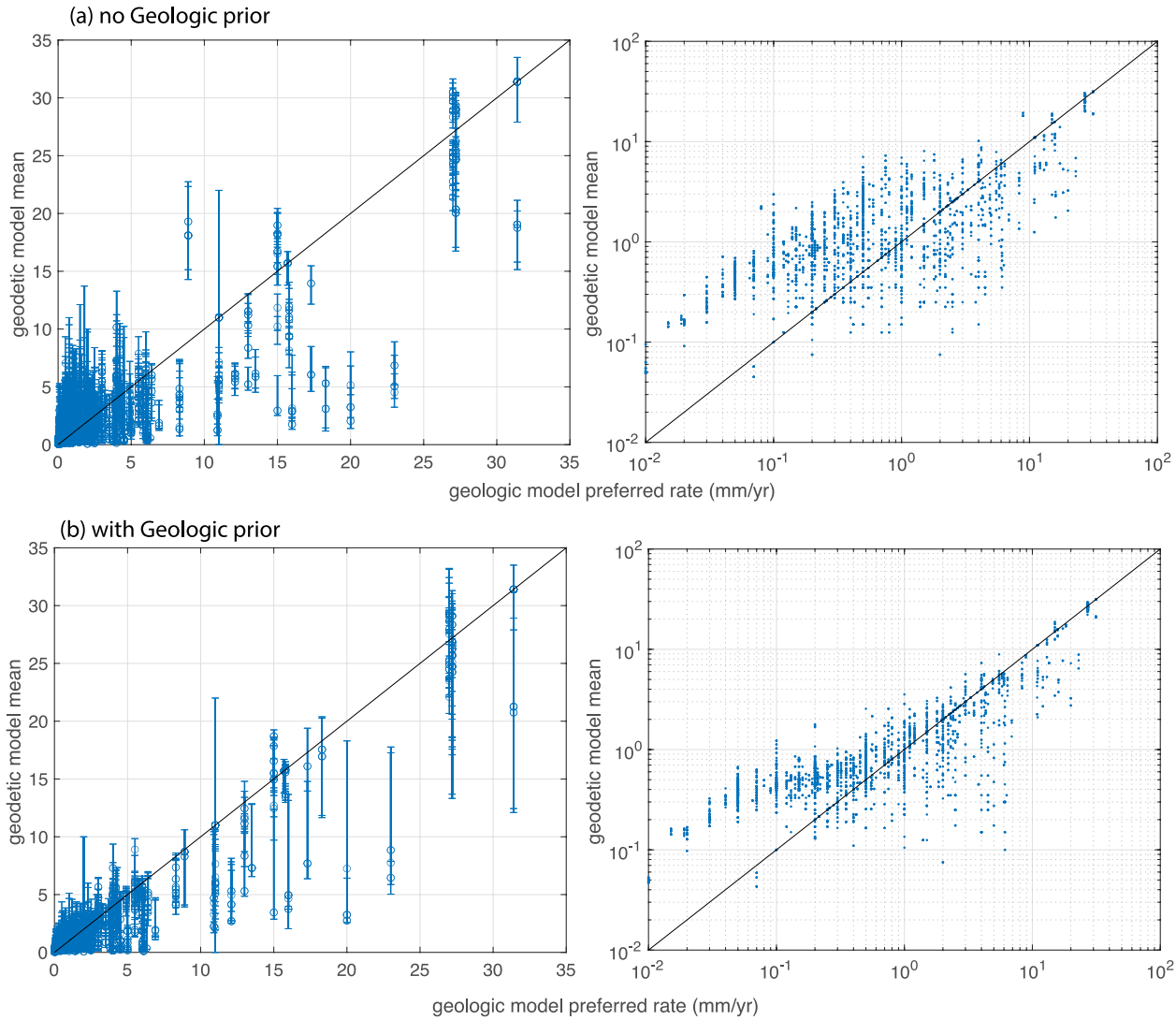

Figure 7. Comparison of Geologic Deformation Model (GDM) preferred slip rates and depth-averaged slip deficit rates. GDM rate is plotted on the horizontal axes and geodetically derived slip deficit rate is plotted on the vertical axes. (a) Geodetic result with no geologic prior. Error bars show the upper and lower 95% confidence limits for the geodetically derived rates. (b) Geodetic result with geologic prior.

However, we note that this section of the Alpine Fault is near the coastline or entirely off shore, and therefore the geodetic data constraints are poor and the computed strain rates here are dependent on the offshore boundary conditions. It is clear from a comparison of the two aggregate model results in Figure 8 that the "Geologic Prior" slip rate estimates are shifted closer to the GDM, and in a majority of fault sections, the 95% confidence regions overlap the geologic model rates. However, even with the geologic prior, the estimated slip deficit rates along the southern sections of the Hope, Wairarapa, and Wellington Faults are lower than the geologic range.

The residual strain rates for the "No Geologic Prior" are analyzed in Figure 9. The strain rate "style" of the mean residual strain rate map is shown in Figure 9a and the NZ NSHM 2022 geologic model faulting style is shown in Figure 9b. Figures 9c and 9d shows the 95% confidence wedges on the orientations of residual principal strain rates. These wedges are computed by subtracting the mean model strain rate field from the combined strain rate field and 95% confidence intervals. Thus, these uncertainties in residual strain rate only incorporate uncertainties in the observed strain rates, not uncertainties in model strain rates. Figures 9c and 9d only shows strain rates at locations where 95% confidence wedge angle is less than 60°. The symbols with red bars or wedges indicate shortening and blue bars/wedges indicating extension rates. The residual strain rates are discussed in more detail in the Discussion section.

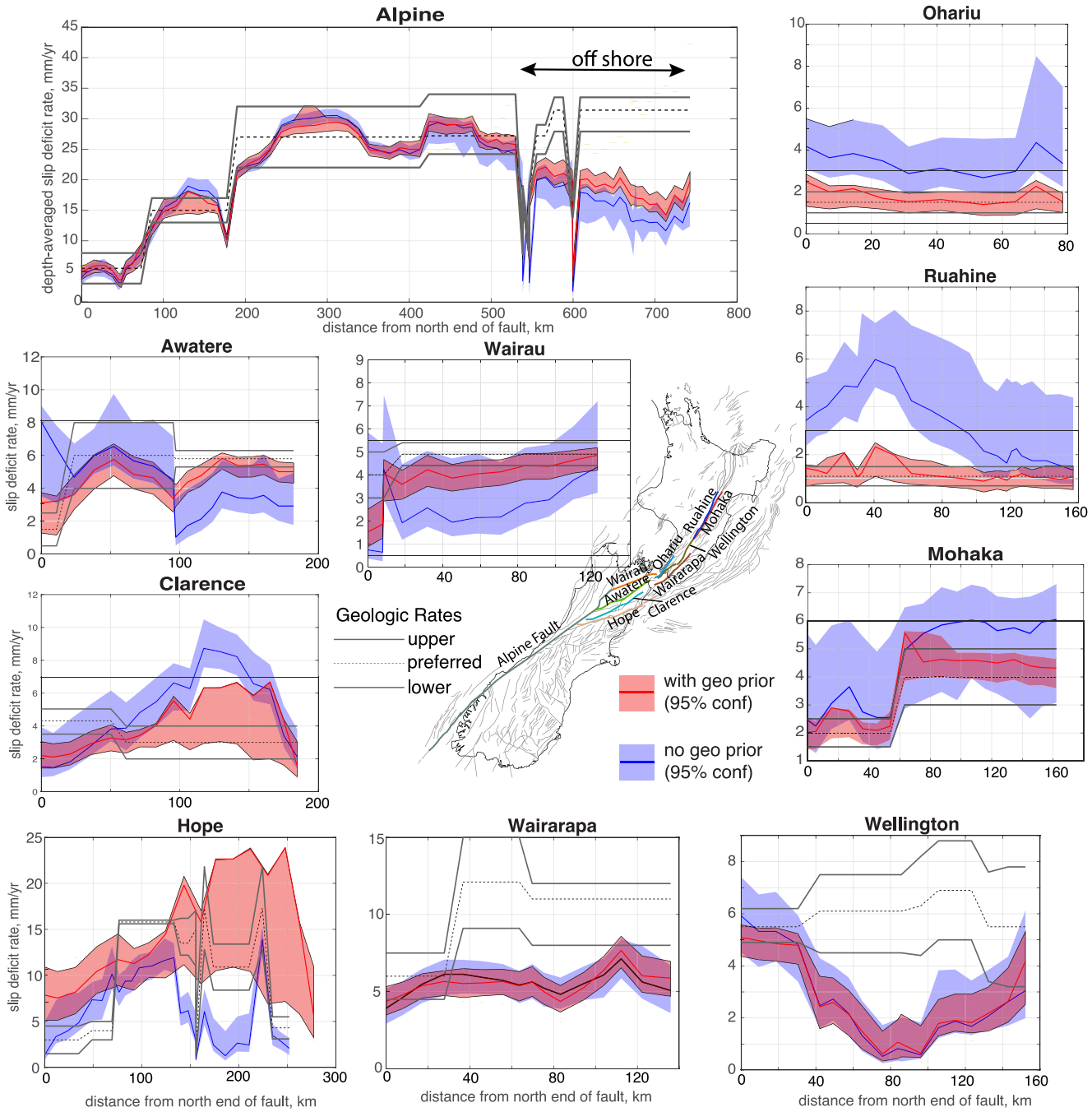

Figure 8. Comparison of along-fault depth-averaged slip deficit rates for inversions with and without the geologic priors. The aggregate distributions shown with solid lines (mean) and red (Geologic Prior) or blue (No Geologic Prior) shading of 95% confidence regions. Geologic deformation model preferred rates (black dashed) and upper and lower bounds (solid black) shown for comparison. See Figure S1 in Supporting Information S1 for similar plots that show results for each of the four strain rate maps.

5. Discussion of Results

Figure 7 shows that on average across the entire New Zealand plate boundary, the geologic model slip rates on low-rate faults with slip rates less than about one mm/yr are systematically lower than the geodetically-inferred slip deficit rates. This could occur for several reasons: (a) if the slip rates on low-rate faults are systematically underestimated in the geologic model, or (b) other low-rate faults are missing in the fault model, or (c) off-fault strain that is not released as slip on faults and is incorrectly mapped to fault slip deficit rate in the geodetic

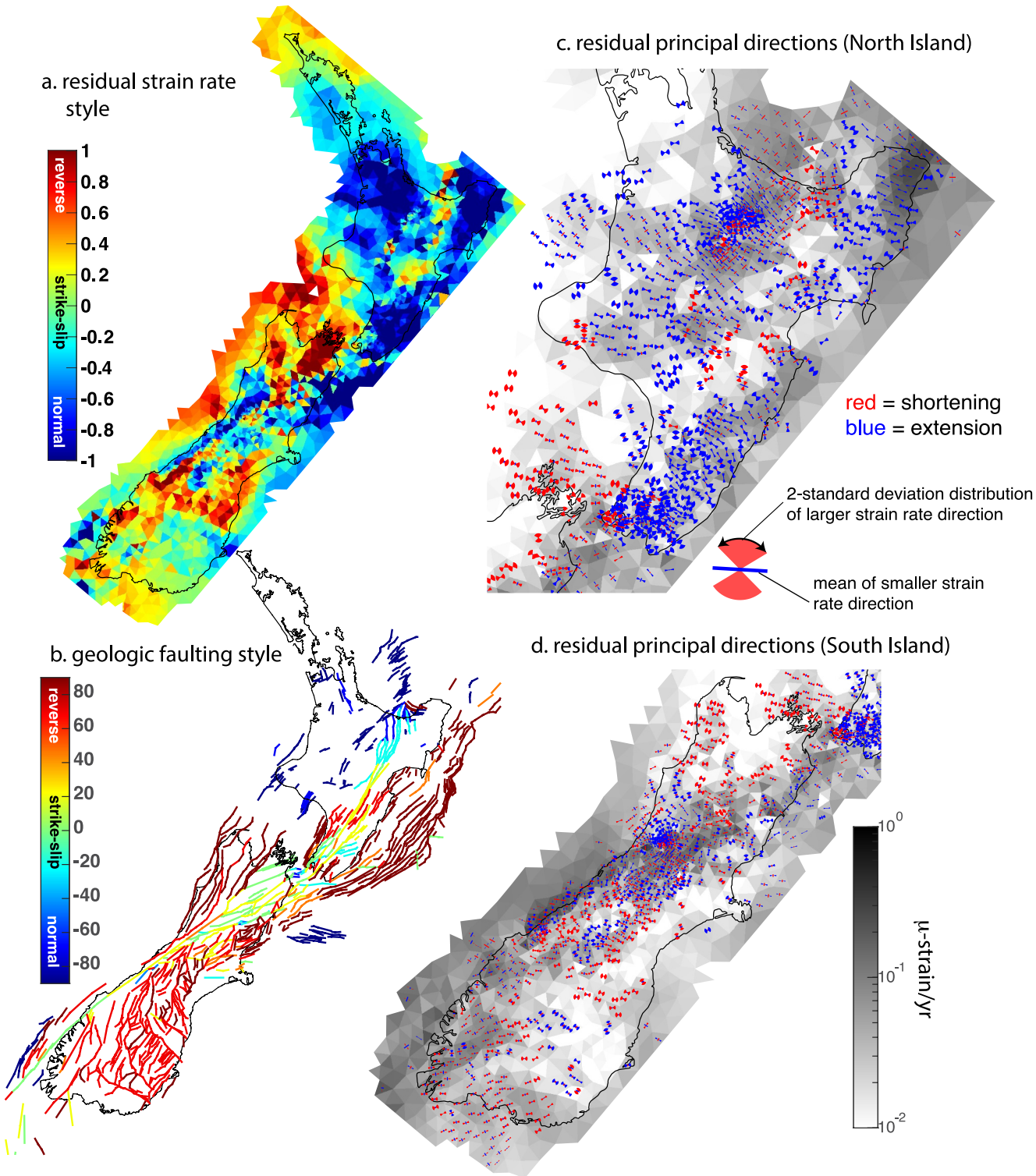

Figure 9. Residual strain rate field computed by subtracting the mean model strain rate field (mean of all inversions) from all observed strain rate map realizations. (a) Residual strain rate style. Style is defined in terms of principal strain rates $(\varepsilon_1 + \varepsilon_2)/(|\varepsilon_1| + |\varepsilon_2|)$, and ranges from −1 (normal faulting) to +1 (reverse fault). (b) Geologic faulting style which defined based on the rake. Color shows angle between rake vector and strike line on the fault plane, without distinguishing sense of strike slip. (c–d) Principal residual strain rate orientations and 95% confidence wedges. Uncertainty wedges are shown for the larger of the absolute values of the two mean principal directions. Color indicates shortening (red) and extension (blue). Gray shading shows residual maximum shear strain rates.

inversion. The systematically lower geodetically derived slip deficit rates on fault sections with slip rates between about 5 and 25 mm/yr could potentially be attributed to fault creep, that is, the present-day slip deficit rate is lower than the long-term slip rate because faults partially creep during the interseismic period. To our knowledge surface creep is not widely observed in New Zealand, so the discrepancy would have to be associated with interseismic creep rates at depth. Alternatively, it is possible that slip rates on some of these fault systems vary temporally (e.g., Bennett, 2007; Zinke et al., 2019) and/or the geological slip rates are systematically overestimated. Further examination of these systematic discrepancies is warranted for future studies.

Despite the suggestion of systematic differences in geodetically derived slip deficit rates and geologic model slip rates illustrated in Figure 7, depth-averaged slip deficit rates agree remarkably well with geologic model slip rates, within uncertainties, along many of the high-rate faults in New Zealand (Figure 8). Along the Alpine fault the slip deficit rates gradually increase along strike from north to south (in both the Geologic Prior and No Geologic Prior inversion), consistent with the geologic slip rates (ignoring the offshore southern section where the geodetic rates are likely underestimates of the true slip deficit rate). This along-strike change in Alpine Fault slip rate is related to slip being fed onto the Marlborough Fault system as those faults intersect the Alpine Fault (Berryman et al., 1992). It is remarkable that the geodetic data is capable of capturing this along-strike change in Alpine Fault slip rate so clearly, even in the model without geological constraints. Previous modeling of geodetic data in the South Island (Wallace et al., 2007) has also captured this along-strike variation in Alpine Fault slip rate, although they utilized a block modeling approach that included the Marlborough faults, so this along-strike variation was effectively imposed by the block kinematic constraints (which is not the case in this model).

This study also provides new insights into potential slip rates on faults within the Main Divide area, a distributed zone of deformation and faulting of the central Southern Alps, to the east of the Alpine Fault (Figure 1). The Main Divide Fault Zone has been postulated to accommodate active deformation although quantifying the rates of deformation the zone might accommodate has not been possible due to a lack of datable offset features (Cox & Findlay, 1995). Wallace et al. (2007) modeled ∼5 mm/yr of distributed deformation across the Main Divide using a deforming block model and geodetic data, although this model did not include individual faults within the Main Divide Fault Zone. Our inversions indicate a total of up to 4–7 mm/yr of oblique slip (right-lateral plus reverse) is accommodated on small faults within the Main Divide Fault Zone, similar to the ∼5 mm/yr of distributed deformation identified by Wallace et al. (2007).

Our model results also help to resolve slip rates on other fault systems in the South Island that are difficult to estimate geologically, such as the reverse faulting domain in the northwestern South Island (NCFS), and the Porters Pass/Amberley Fault Zone of northern Canterbury (See Figure 1 for locations). Our geodetic inversion results indicate summed geodetic slip rates across the NCFS region are 2–5 mm/yr faster than ∼1 mm/yr geologic summed across this region that hosted 1929 M7.3 Buller earthquake and the M7.1 1969 Inangahua earthquake (see faster geodetic rates in Figure 6 in northwest corner of South Island). Reverse-style residual strain rates at ∼20 nano-strain/year across this region add to the total model deformation across the NCFS. Similar to the Main Divide Fault Zone, geological estimates of slip rates for these bedrock faults are difficult to obtain due to a lack of datable offset features, and the geodetic models provide unique information about their rates of deformation. Likewise, the complexly deforming Porters Pass-Amberley Fault Zone in northern Canterbury (north of Christchurch) is characterized by a distributed region of folding and oblique transpression (Pettinga et al., 2001), making estimates of long-term deformation rates inherently difficult. Wallace et al. (2007) suggested that geodetic rates of deformation (∼6–7 mm/yr of dextral transpression) within the Porters-Pass Amberley Fault Zone were higher than previously estimated geological rates of ∼2 mm/yr (Cowan et al., 1996; Pettinga et al., 2001). Our inversion results indicate 3–6 mm/yr of slip summed across this zone, which is 2–4 mm/yr higher than in the geologic model (see Figure 6).

Across the Marlborough Fault System, the slip deficit rates are largely in agreement with the geologic model slip rates although the slip deficit rates on the Wairarapa Fault tend to be at the low end or lower than the geologic range, and conversely on the southern part of the Clarence fault the geodetically-derived slip deficit rates tend toward the high end or higher than the geologic range. Zinke et al. (2019) utilized faulted river terraces spanning the Clarence Fault at point on the southern half of the fault to reveal a nearly five-fold variation in slip rates (2–9.6 mm/yr) through the Holocene and late Pleistocene period, which varied systematically with slip rates on the southern half of the Awatere fault, suggesting that the slip rates on the two fault systems are anti-correlated in time (slip on faults trade off with time). Our estimated slip rates on the southern portion of the Clarence fault are

comparable to the slip rates in the fastest period obtained by Zinke et al. (2019), and our estimated slip rates on the southern Awatere Fault are at or below the low end of the geological range. This relationship between present-day Awatere and Clarence fault slip rates and the geologic average rates is consistent with anticorrelation inferred by Zinke et al. (2019). Our estimated Hope Fault slip deficit rates are lower than the geological rates (Figure 9) for the inversion without the geologic prior, suggesting the possibility that the Hope Fault slip rates may also trade-off temporally with Clarence Fault. One cautionary note is that we estimate slip deficit rate, not total slip rate, so slip deficit rates that are lower than the geologic rates could be indicative of low interseismic fault coupling. Furthermore, slip rates on closely spaced faults (within about two locking depths, or about 30–40 km) such as the Marlborough Fault System will be inherently correlated, leading to potential trade-offs between fault slip rates that are not related to temporal variability.

To the northeast of the MFS, the geodetically derived slip deficit rates across the southern part of the NIFS are significantly lower than the geologic slip rates. The slip deficit rates on the southern 100–120 km sections of the Wairarapa and Wellington faults are as much as 5 mm/yr lower than the geologic slip rates. This result has particularly important implications for hazard in the populated Wellington region. Wallace et al. (2004) also obtained slip rates for the Wairarapa Fault that were somewhat lower than geological estimates (7–8 mm/yr vs. 10–12 mm/yr). The slip deficit rates on the northern part of the NIFS are generally consistent with the geologic slip rates on the Mohaka and Ohariu Faults, however the slip deficit rates in the No Geologic Prior inversion are roughly a factor of two higher than the geologic rates on the Ohariu Fault. This suggests the possibility that there could be some trade-off in slip rate with time for the nearby Ohariu and Wellington Faults, similar to what is observed from paleoseismic data for the Clarence and Awatere Faults in Marlborough.

It is not clear why the slip deficit rates on the Wairarapa and Wellington faults are clearly lower than the geologic slip rates. We conducted test inversions in which we encouraged slip deficit rates on these faults to approach the geologic slip rates and we found it was not possible to fit the strain rate data with such high slip rates; the observed strain rates in this region are not consistent with slip deficit at the higher geologic rates. Wallace et al. (2004) also had difficulty fitting the geological rates for these faults in their block model of the geodetic velocities in the North Island, and they implemented tight geological constraints for these faults—models that they undertook with no geologic constraints also produced lower rates for the Wellington and Wairarapa Faults. One possible explanation is that interseismic fault creep is relatively higher along these faults (and thus slip deficit is lower than long-term slip rate). However, at these high slip rates we would expect widespread interseismic creep to be observable with surface offsets, but no surface creep is observed in this region. Another possibility is that the present-day slip rates along these faults are indeed lower than the long-term slip rates observed in the geology, as discussed above. It is important to note that the strain maps we use have already removed the elastic strain due to Hikurangi subduction interface coupling. It is possible that there are some model trade-offs between Hikurangi subduction slip deficits and upper plate faulting slip rates, that could be leading to the lower geodetic estimates of Wellington and Wairarapa Fault slip rates in the models presented here. We plan to jointly invert the strain rate field for Hikurangi interface and upper plate fault slip deficit rates in future work to address the possible impact of this.

It is clear from Figure 9 that the residual strain rates are not simply random noise; there are clear spatial patterns in residual strain rate style and orientations. For example, the predominant residual strain rate field throughout the North Island is normal-faulting style with maximum extension rate directions oriented predominantly in the NW-SE quadrants. The northern third of South Island is predominantly reverse-faulting style residual strain rates. Along zones surrounding the Alpine Fault and within the Southland and Otago regions, there are zones of either reverse or normal-faulting style. The spatial distribution of residual strain rate style is similar to the geologic faulting style in the NCFS and in areas of the contractional belts in the Otago region. Residual extensional strain rate style west of the NIFS is consistent with geologic intra-arc and back-arc normal faulting. Geodetically-derived normal-faulting style along the eastern coastline of the North Island where deformation is influenced by coupling on the Hikurangi Subduction zone is not consistent with the reverse faulting in the geologic model. This is likely due to the fact that the interseismic coupling model was subtracted from the geodetic velocity field that was used to compute the four NZ NSHM 2022 strain rate maps. It is likely that the model over-predicts the amount of contractional strain in this region caused by the subduction interface, and in future work we plan to jointly invert for Hikurangi interface slip deficits and upper plate faulting sources. However, we note that there are some areas of geodetic extension along the east coast of the North Island in strain rate models without the subduction interface coupling removed, within the Raukumara Peninsula of the northeastern North Island, and just to the south of Hawkes Bay (Dimitrova et al., 2016; Haines & Wallace, 2020). Dimitrova et al. (2016)

suggested that those areas of relatively localized extension coincides with areas of normal faulting and/or deep-seated landsliding. Nearly alternating pockets of normal and reverse-sense residual faulting-style within the strike slip Alpine-Marlborough Fault systems is not easily reconcilable with the geologic model that shows trans-pressional faulting (strike-slip with an oblique reverse sense).

The interpretation of the residual strain rate field is not straightforward. Whether the residual strain rate field is in reality accommodated by slip deficit on faults not in the model, or as distributed inelastic off-fault strain throughout the crust is not known from this study. Laboratory studies (e.g., Chaipornkaew et al., 2022), field studies (e.g., Goren et al., 2015; Gray et al., 2017; Shelef & Oskin, 2010), and numerical models (e.g., Herbert et al., 2014; Bird, 2009a) indicate that a sizable portion (~10%–30%) of deformation can occur off main faults. Thus it is possible that a portion of the geodetic moment rate is not released by slip on faults and instead manifests as distributed inelastic deformation through the crust. It is possible that these pockets of residual deformation that do not match the geologic faulting style could be attributed to mis-modeling of fault rake, which is fixed to the geologic model, but this would require further testing to evaluate. It is also possible that some of the residual strain rate inferred in this study could be attributed to other deficient features of the model. For example, elastic heterogeneity in the crust (e.g., Williams & Wallace, 2015) and time-dependent strain rates due to earthquake cycle mantle flow (e.g., Chuang & Johnson, 2011; Hearn et al., 2013; Li et al., 2018) are not modeled in this study. Future work should consider such effects.

Several results from this study have implications for active deformation in other plate boundaries around the world. Similar to this study, deformation models for the Western US National Seismic Hazard Model (Pollitz et al., 2022) show a tendency for geodetically-derived slip rates on faults with slip rates below 1 mm/yr to be higher than geologic estimates and Johnson (2023, manuscript in revision, JGR) similarly shows that geodetically-derived moment rates in lower deforming rate regions in the western US are higher than geologic rates. This suggests the systematic discrepancy may not be just limited to the tectonic setting in New Zealand. The Western US deformation models (Pollitz et al., 2022) were designed to fit surface velocities rather than strain rates, so the discrepancies appear in analyses of velocities as well as strain rates.

While there are notable differences between present-day geodetic slip deficit rates and geologically-determined slip rates along the Wellington and Wairarapa faults, it is noteworthy that the vast majority of geodetic slip deficit rates in this study agree to within uncertainties with geologic slip rates. Worldwide, a number of discrepancies between geologic and geodetic slip deficit rates have been identified (e.g., Dolan & Meade, 2017). Some discrepancies have been attributed by authors to be a result of mis-modeling of time-dependent deformation at different times of the earthquake cycle (e.g., Chuang & Johnson, 2011; Hearn et al., 2013; Tong et al., 2014; Dolan & Meade, 2017) while other studies suggest that actual variations in slip rates on faults over time can account for the discrepancies (e.g., Bennett, 2007; Oskin et al., 2008). Time-dependence of slip rates and surface deformation rates should be examined carefully in future studies of slip deficit rates in New Zealand.

6. Conclusions

We develop a new approach for inverting for crustal fault slip rates within complexly deforming tectonic zones with an application to the New Zealand plate boundary. The method inverts strain rates (rather than velocity fields) for slip deficit rates. To capture the epistemic uncertainty introduced by different approaches to obtain strain rates from GNSS velocity fields, we conducted four inversions for slip deficit rate for four different strain rate maps (utilizing different approaches to estimating strain), for a total of 16 inversions. We find that about 70%–80% of the total strain rate field can be explained as elastic strain due to coupling on faults in the New Zealand community fault model. The remaining (residual) strain rates comprising of 20%–30% of the total strain rate field are relatively low in magnitude with maximum shear strain rates typically well below 0.1 micro-strain/yr, yet the residual strain rates are not randomly distributed; there are systematic spatial patterns to the style of the residual strain rates indicating a potential tectonic origin. Future studies should be directed toward identifying the source of the unmodeled strain rates and determine if this unmodeled strain can be attributed to slip deficit on faults not in the model, off-fault strain distributed through the crust, or shortcomings in the modeling.

Slip deficit rates along the on-shore sections of the Alpine Fault are in good agreement with geologic estimates including a gradual increase in slip rate and slip deficit rate along strike from north to south. This gradient in slip rate is apparently related to the partitioning of plate motion by slip onto multiple faults in Marlborough Fault system to the north. Although there is overall good agreement between the geologic preferred rates and the

inverted geodetic slip deficit rates across most faults in New Zealand, there are small and systematic differences that are noteworthy. For faults slipping less that about 1 mm/yr, the geodetically-derived slip deficit rates are systematically higher than the geologic model slip rates. The geodesy-based inversions infer systematically higher slip deficit rates within the Main Divide Fault Zone of the central Southern Alps, the contractional zone in the northwestern South Island that has hosted historical major earthquakes, and within the Porters Pass-Amberley Fault Zone in northern Canterbury. The geodetic rates are systematically lower along the nearshore part of the Hikurangi margin. It is unclear whether these small but systematic discrepancies is a bias in the geodetic inversion results or in the preferred geologic slip rates.

The inversions without geologic priors yield slip deficit rates that are significantly different from the geologic model slip rates along a few of the high rate faults in New Zealand. Inferred slip deficit rates are higher than the geologic model along the Ohariu, Ruahine and southern Clarence Faults. Inferred slip deficit rates are lower than the geologic model along the Hope, Wairarapa, and Wellington Faults. The inversions with geologic priors yield sip deficit rates with 95% confidence limits that largely overlap the range of slip rates in the geologic slip rate model. Three exceptions are the southern section of the Hope fault, the Wairarapa Fault, and the southern sections of the Wellington Fault, all with slip deficit rates at or below the lower limit of the geologic model. It is plausible that these results indicate temporal variation in slip rates on these fault systems or the slip deficit rates may reflect temporal variations in the strain rate field due to time-dependent postseismic and interseismic deformation processes. Further study should be directed at resolving these apparent slip rate discrepancies.

Data Availability Statement

The New Zealand Community Fault model used for the modeling in this study are available via the GNS Science Data Catalogue record at https://doi.org/10.21420/NMSX-WP67 (Seebeck et al., 2022). The New Zealand strain rate maps used in the inversions available for download from a public repository (Maurer (2023), https://osf.io/rgpfe/). The code used to invert strain rate for slip deficit rate is publicly available as a GitHub repository (Johnson (2023b), https://github.com/kajjohns/SliDeFS/tree/v1.0.0). The outputs of the inversions presented in this paper (slip deficit rate realizations for eight inversions) are available for download in a Zenodo repository (Johnson (2023a), https://zenodo.org/records/8132661).

Acknowledgments
The authors thank John Townend (Victoria University of Wellington, NZ), Jessica Murray (United States Geological Survey), and Ned Field (United States Geological Survey) for providing insightful reviews of an early version of this manuscript. This work was funded by the New Zealand Ministry of Business, Innovation, and Employment for GNS Science via the National Seismic Hazard Model 2022 Revision Project (Contract: 2020-BD101).

References

Beanland, S., & Haines, J. (1998). The kinematics of active deformation in the North Island, New Zealand, determined from geological strain rates. *New Zealand Journal of Geology and Geophysics*, *41*(4), 311–323. https://doi.org/10.1080/00288306.1998.9514813

Beavan, J., & Haines, J. (2001). Contemporary horizontal velocity and strain rate fields of the Pacific-Australian plate boundary zone through New Zealand. *Journal of Geophysical Research*, *106*(B1), 741–770. https://doi.org/10.1029/2000JB900302

Beavan, J., Moore, M., Pearson, C., Henderson, M., Parsons, B., Bourne, S., et al. (1999). Crustal deformation during 1994–1998 due to oblique continental collision in the central Southern Alps, New Zealand, and implications for seismic potential of the Alpine fault. *Journal of Geophysical Research*, *104*(B11), 25233–25255. https://doi.org/10.1029/1999JB900198

Beavan, J., Wallace, L. M., Palmer, N., Denys, P., Ellis, S., Fournier, N., et al. (2016). New Zealand GPS velocity field: 1995–2013. *New Zealand Journal of Geology and Geophysics*, *59*(1), 5–14. https://doi.org/10.1080/00288306.2015.1112817

Bennett, R. A. (2007). Instantaneous slip rates from geology and geodesy. *Geophysical Journal International*, *169*(1), 19–28. https://doi.org/10.1111/j.1365-246X.2007.03331.x

Berryman, K., Beanland, S., Cooper, A., Cutten, H., Norris, R., & Wood, P. (1992). *The Alpine Fault, New Zealand: Variation in Quaternary structural style and geomorphic expression* (pp. 126–163). Annales Tectonicae, VI.

Bird, P. (2009a). Long-term fault slip rates, distributed deformation rates, and forecast of seismicity in the western United States from joint fitting of community geologic, geodetic, and stress direction data sets. *Journal of Geophysical Research*, *114*(B11), B11403. https://doi.org/10.1029/2009JB006317

Bird, P. (2009b). Long-term fault slip rates, distributed deformation rates, and forecast of seismicity in the western United States from joint fitting of community geologic, geodetic, and stress direction data sets. *Journal of Geophysical Research*, *114*(B11), B11403. https://doi.org/10.1029/2009jb006317

Bird, P., Jackson, D. D., Kagan, Y. Y., Kreemer, C., & Stein, R. S. (2015). GEAR1: A global earthquake activity rate model constructed from geodetic strain rates and smoothed seismicity. *Bulletin of the Seismological Society of America*, *105*(5), 2538–2554. https://doi.org/10.1785/0120150058

Chaipornkaew, L., Elston, H., Cooke, M., Mukerji, T., & Graham, S. A. (2022). Predicting off-fault deformation from experimental strike-slip fault images using convolutional neural networks. *Geophysical Research Letters*, *49*(2), e2021GL096. https://doi.org/10.1029/2021GL096854

Chuang, R. Y., & Johnson, K. (2011). Reconciling geologic and geodetic model fault slip-rate discrepancies in Southern California: Consideration of nonsteady mantle flow and lower crustal fault creep. *Geology*, *39*(7), 627–630. https://doi.org/10.1130/g32120.1

Cowan, H., Nicol, A., & Tonkin, P. (1996). A comparison of historical and paleoseismicity in a newly formed fault zone and a mature fault zone, North Canterbury, New Zealand. *Journal of Geophysical Research*, *101*(B3), 6021–6036. https://doi.org/10.1029/95JB01588

Cox, S. C., & Findlay, R. H. (1995). The main divide fault zone and its role in formation of the Southern Alps, New Zealand. *New Zealand Journal of Geology and Geophysics*, *38*(4), 489–499. https://doi.org/10.1080/00288306.1995.9514675

Dimitrova, L., Wallace, L., Haines, A., & Williams, C. (2016). High-resolution view of active tectonic deformation along the Hikurangi subduction margin and the Taupo Volcanic Zone, New Zealand. *New Zealand Journal of Geology and Geophysics*, *59*(1), 43–57. https://doi.org/10.1080/00288306.2015.1127823

Dolan, J. F., & Meade, B. J. (2017). A comparison of geodetic and geologic rates prior to large strike-slip earthquakes: A diversity of earthquake-cycle behaviors? *Geochemistry, Geophysics, Geosystems*, *18*(12), 4426–4436. https://doi.org/10.1002/2017GC007014

Engwirda, D. (2014). *Locally-optimal Delaunay-refinement and optimisation-based mesh generation PhD Thesis*. The University of Sydney, School of Mathematics and Statistics.

Evans, E. L. (2022). A dense block model representing western continental United States deformation for the 2023 Update to the national seismic hazard model. *Seismological Research Letters*, *93*(6), 3024–3036. https://doi.org/10.1785/0220220141

Evans, E. L., Loveless, J. P., & Meade, B. J. (2015). Total variation regularization of geodetically and geologically constrained block models for the Western United States. *Geophysical Journal International*, *202*(2), 713–727.

Field, E. H., Arrowsmith, R. J., Biasi, G. P., Bird, P., Dawson, T. E., Felzer, K. R., et al. (2014). Uniform California Earthquake Rupture Forecast version 3 (UCERF3): The time-independent model. *Bulletin of the Seismological Society of America*, *104*, 1122–1180. https://doi.org/10.1785/0120130164

Fukahata, Y., & Wright, T. J. (2008). A non-linear geodetic data inversion using ABIC for slip distribution on a fault with an unknown dip angle. *Geophysical Journal International*, *173*(2), 353–364. https://doi.org/10.1111/j.1365-246X.2007.03713.x

Fukuda, J., & Johnson, K. M. (2008). A fully Bayesian inversion for spatial distribution of fault slip with objective smoothing. *Bulletin of the Seismological Society of America*, *98*(3), 1128–1146. https://doi.org/10.1785/0120070194

Goren, L., Castelltort, S., & Klinger, Y. (2015). Modes and rates of horizontal deformation from rotated river basins: Application to the Dead Sea fault system in Lebanon. *Geology*, *43*(9), 843–846. https://doi.org/10.1130/G36841.1

Gray, H. J., Shobe, C. M., Hobley, D. E., Tucker, G. E., Duvall, A. R., Harbert, S. A., & Owen, L. A. (2017). Off-fault deformation rate along the southern San Andreas fault at Mecca Hills, southern California, inferred from landscape modeling of curved drainages. *Geology*, *46*(1), 59–62. https://doi.org/10.1130/G39820.1

Haines, A. J., Dimitrova, L. L., Wallace, L. M., & Williams, C. A. (2015). Introduction to the Vertical Derivatives of Horizontal Stress (VDoHS) rates. In A. J. Haines, L. L. Dimitrova, L. M. Wallace, & C. A. Williams (Eds.), *Enhanced surface imaging of crustal deformation: Obtaining tectonic force fields using GPS data*, *Springer briefs in Earth sciences* (pp. 9–18). Springer International Publishing. https://doi.org/10.1007/978-3-319-21578-5_2

Haines, A. J., & Wallace, L. M. (2020). New Zealand-wide geodetic strain rates using a physics-based approach. *Geophysical Research Letters*, *47*(1), e2019GL084. https://doi.org/10.1029/2019GL084606

Hammond, W. C., Blewitt, G., & Kreemer, C. (2011). Block modeling of crustal deformation of the northern Walker Lane and Basin and Range from GPS velocities. *Journal of Geophysical Research*, *116*(B4), B04402. https://doi.org/10.1029/2010jb007817

Hearn, E. H., Pollitz, F. F., Thatcher, W. R., & Onishi, C. T. (2013). How do "ghost transients" from past earthquakes affect GPS slip rate estimates on southern California faults? *Geochemistry, Geophysics, Geosystems*, *14*(4), 828–838. https://doi.org/10.1002/ggge.20080

Herbert, J. W., Cooke, M. L., Oskin, M., & Difo, O. (2014). How much can off-fault deformation contribute to the slip rate discrepancy within the eastern California shear zone? *Geology*, *42*(1), 71–75. https://doi.org/10.1130/G34738.1

Herman, M. W., & Govers, R. (2020). Locating fully locked asperities along the south America subduction megathrust: A new physical interseismic inversion approach in a Bayesian framework. *Geochemistry, Geophysics, Geosystems*, *21*(8), e2020GC009. https://doi.org/10.1029/2020GC009063

Holt, W. E., & Haines, A. J. (1995). The kinematics of northern South Island, New Zealand, determined from geologic strain rates. *Journal of Geophysical Research*, *100*(B9), 17991–18010. https://doi.org/10.1029/95JB01059

Jiang, Y., Samsonov, S. V., & González, P. J. (2022). Aseismic fault slip during a shallow normal-faulting seismic swarm constrained using a physically informed geodetic inversion method. *Journal of Geophysical Research: Solid Earth*, *127*(7), e2021JB022. https://doi.org/10.1029/2021JB022621

Johnson, K. (2023a). Slip deficit rate realizations for 2023 New Zealand national seismic hazard model geodetic inversions [Dataset]. Zenodo. https://doi.org/10.5281/zenodo.8132661

Johnson, K. M. (2023b). SliDeFS v1.0.0 [Software]. Zenodo. https://doi.org/10.5281/zenodo.8131992

Johnson, K. M., & Fukuda, J. (2010). New methods for estimating the spatial distribution of locked asperities and stress-driven interseismic creep on faults with application to the San Francisco Bay Area, California. *Journal of Geophysical Research*, *115*(B12), B12408. https://doi.org/10.1029/2010jb007703

Johnson, K. M., Wallace, L. M., Maurer, J., Hamling, I. J., Williams, C. A., Rollins, C., et al. (2022). Geodetic deformation model for the 2022 update of the New Zealand national seismic hazard model. https://doi.org/10.21420/P93X-8293

Kreemer, C., Holt, W. E., Goes, S., & Govers, R. (2000). Active deformation in eastern Indonesia and the Philippines from GPS and seismicity data. *Journal of Geophysical Research*, *105*(B1), 663–680. https://doi.org/10.1029/1999jb900356

Kreemer, C., Holt, W. E., & Haines, A. J. (2002). The global moment rate distribution within plate boundary zones. In *Plate boundary zones* (pp. 173–190). American Geophysical Union (AGU). https://doi.org/10.1029/GD030p0173

Kreemer, C., & Young, Z. M. (2022). Crustal strain rates in the western United States and their relationship with earthquake rates. *Seismological Research Letters*, *93*(6), 2990–3008. https://doi.org/10.1785/0220220153

Li, S., Wang, K., Wang, Y., Jiang, Y., & Dosso, S. E. (2018). Geodetically inferred locking state of the Cascadia megathrust based on a viscoelastic Earth model. *Journal of Geophysical Research: Solid Earth*, *123*(9), 8056–8072. https://doi.org/10.1029/2018JB015620

Matthews, M. V., & Segall, P. (1993). Estimation of depth-dependent fault slip from measured surface deformation with application to the 1906 San Francisco Earthquake. *Journal of Geophysical Research*, *98*(B7), 12153–12163. https://doi.org/10.1029/93JB00440

Maurer, J. (2023). New Zealand strain rates [Dataset]. OSF. https://doi.org/10.17605/OSF.IO/RGPFE

Maurer, J., Johnson, K., Wallace, L. M., Hamling, I., Williams, C. A., Rollins, C., et al. (2023). Geodetic strain rates for the 2022 update of the New Zealand national seismic hazard model. *Bulletin of the Seismological Society of America*, *114*(1), 57–77. https://doi.org/10.1785/0120230145

Maurer, J., & Materna, K. (2023). Quantification of geodetic strain rate uncertainties and implications for seismic hazard estimates. *Geophysical Journal International*, *234*(3), 2128–2142. https://doi.org/10.1093/gji/ggad191

Mazzotti, S., Leonard, L., Cassidy, J., Rogers, G., & Halchuk, S. (2011). Seismic hazard in western Canada from GPS strain rates versus earthquake catalog. *Journal of Geophysical Research*, *116*(B12), B12310. https://doi.org/10.1029/2011jb008213

Mazzotti, S., Le Pichon, X., Henry, P., & Miyazaki, S.-I. (2000). Full interseismic locking of the Nankai and Japan-west Kurile subduction zones: An analysis of uniform elastic strain accumulation in Japan constrained by permanent GPS. *Journal of Geophysical Research*, *105*(B6), 13159–13177. https://doi.org/10.1029/2000JB900060

McCaffrey, R. (2005). Block kinematics of the Pacific-North America plate boundary in the southwestern United States from inversion of GPS, seismological, and geologic data. *Journal of Geophysical Research*, *110*(B7), B07401. https://doi.org/10.1029/2004JB003307

Meade, B. J., & Hager, B. H. (2005). Block models of crustal motion in southern California constrained by GPS measurements. *Journal of Geophysical Research*, *110*(B3), B03403. https://doi.org/10.1029/2004JB003209

Minson, S. E., Simons, M., & Beck, J. L. (2013). Bayesian inversion for finite fault earthquake source models I—Theory and algorithm. *Geophysical Journal International*, *194*(3), 1701–1726. https://doi.org/10.1093/gji/ggt180

Mosegaard, K., & Tarantola, A. (1995). Monte Carlo sampling of solutions to inverse problems. *Journal of Geophysical Research*, *100*(B7), 12431–12447. https://doi.org/10.1029/94JB03097

Okada, Y. (1992). Internal deformation due to shear and Tensile Faults in a half-space. *Bulletin of the Seismological Society of America*, *82*(2), 1018–1040. https://doi.org/10.1785/bssa0820021018

Oskin, M., Perg, L., Shelef, E., Strane, M., Gurney, E., Singer, B., & Zhang, X. (2008). Elevated shear zone loading rate during an earthquake cluster in eastern California. *Geology*, *36*(6), 507–510. https://doi.org/10.1130/G24814A.1

Petersen, M. D., Moschetti, M. P., Powers, P. M., Mueller, C. S., Haller, K. M., Frankel, A. D., et al. (2014). Documentation for the 2014 update of the United States national seismic hazard maps, USGS Numbered Series 2014-1091. In *Code Number: 2014-1091 Code: Documentation for the 2014 update of the United States national seismic hazard maps Publication Title: Documentation for the 2014 update of the United States national seismic hazard maps Reporter: Documentation for the 2014 update of the United States national seismic hazard maps Series: Open-File Report IP-052282*. U.S. Geological Survey. https://doi.org/10.3133/ofr20141091

Pettinga, J. R., Yetton, M. D., Van Dissen, R. J., & Downes, G. (2001). Earthquake source identification and characterisation for the Canterbury region, South Island, New Zealand. *Bulletin of the New Zealand Society for Earthquake Engineering*, *34*(4), 282–317. https://doi.org/10.5459/bnzsee.34.4.282-317

Pollitz, F. F., Evans, E. L., Field, E. H., Hatem, A. E., Hearn, E. H., Johnson, K., et al. (2022). Western U.S. Deformation models for the 2023 update to the U.S. National seismic hazard model. *Seismological Research Letters*, *93*(6), 3068–3086. https://doi.org/10.1785/0220220143

Pollitz, F. F., McCrory, P., Svarc, J., & Murray, J. (2008). Dislocation models of interseismic deformation in the western United States. *Journal of Geophysical Research*, *113*(B4), B04413. https://doi.org/10.1029/2007JB005174

Rastin, S. J., Rhoades, D. A., Rollins, C., & Gerstenberger, M. C. (2022). How useful are strain rates for estimating the long-term spatial distribution of earthquakes? *Applied Sciences*, *12*(13), 6804. https://doi.org/10.3390/app12136804

Rhoades, D., Christophersen, A., & Gerstenberger, M. (2017). Multiplicative earthquake likelihood models incorporating strain rates. *Geophysical Journal International*, *208*(3), 1764–1774. https://doi.org/10.1093/gji/ggw486

Savage, J. C. (1983). A dislocation model of strain accumulation and release at a subduction zone. *Journal of Geophysical Research*, *88*(B6), 4984–4996. https://doi.org/10.1029/jb088ib06p04984

Savage, J. C., & Burford, R. O. (1970). Accumulation of tectonic strain in California. *Bulletin of the Seismological Society of America*, *60*(6), 1877–1896. https://doi.org/10.1785/BSSA0600061877

Savage, J. C., & Simpson, R. W. (1997). Surface strain accumulation and the seismic moment tensor. *Bulletin of the Seismological Society of America*, *87*(5), 1345–1353. https://doi.org/10.1785/bssa0870051345

Seebeck, H., Dissen, R. V., Litchfield, N., Barnes, P. M., Nicol, A., Langridge, R., et al. (2023). The New Zealand community fault model – Version 1.0: An improved geological foundation for seismic hazard modelling. *New Zealand Journal of Geology and Geophysics*, *0*(0), 1–21. https://doi.org/10.1080/00288306.2023.2181362

Seebeck, H., Van Dissen, R., Litchfield, N., Barnes, P., Nicol, A., Langridge, R., et al. (2022). New Zealand Community Fault Model – version 1.0 [Dataset]. GNS Science Dataset Catalogue. https://doi.org/10.21420/NMSX-WP67

Shelef, E., & Oskin, M. (2010). Deformation processes adjacent to active faults: Examples from eastern California. *Journal of Geophysical Research*, *115*(B5), B05308. https://doi.org/10.1029/2009JB006289

Tong, X., Smith-Konter, B., & Sandwell, D. T. (2014). Is there a discrepancy between geological and geodetic slip rates along the San Andreas Fault System? *Journal of Geophysical Research: Solid Earth*, *119*(3), 2518–2538. https://doi.org/10.1002/2013JB010765

Van Dissen, R., & Yeats, R. S. (1991). Hope fault, Jordan thrust, and uplift of the Seaward Kaikoura range, New Zealand. *Geology*, *19*(4), 393–396. https://doi.org/10.1130/0091-7613(1991)019¡0393:HFJTAU¿2.3.CO;2

Wallace, L. M., Beavan, J., Bannister, S., & Williams, C. (2012). Simultaneous long-term and short-term slow slip events at the Hikurangi subduction margin, New Zealand: Implications for processes that control slow slip event occurrence, duration, and migration. *Journal of Geophysical Research*, *117*(B11), B11402. https://doi.org/10.1029/2012JB009489

Wallace, L. M., Beavan, J., McCaffrey, R., Berryman, K., & Denys, P. (2007). Balancing the plate motion budget in the South Island, New Zealand using GPS, geological and seismological data. *Geophysical Journal International*, *168*(1), 332–352. https://doi.org/10.1111/j.1365-246X.2006.03183.x

Wallace, L. M., Beavan, J., McCaffrey, R., & Darby, D. (2004). Subduction zone coupling and tectonic block rotations in the North Island, New Zealand. *Journal of Geophysical Research*, *109*(B12), B12406. https://doi.org/10.1029/2004JB003241

Wang, H., & Wright, T. J. (2012). Satellite geodetic imaging reveals internal deformation of western Tibet. *Geophysical Research Letters*, *39*(7), L07303. https://doi.org/10.1029/2012GL051222

Ward, S. N. (1998). On the consistency of earthquake moment rates, geological fault data, and space geodetic strain: The United States. *Geophysical Journal International*, *134*(1), 172–186. https://doi.org/10.1046/j.1365-246x.1998.00556.x

Weiss, J. R., Walters, R. J., Morishita, Y., Wright, T. J., Lazecky, M., Wang, H., et al. (2020). High-resolution surface velocities and strain for Anatolia from Sentinel-1 InSAR and GNSS data. *Geophysical Research Letters*, *47*(17), e2020GL087. https://doi.org/10.1029/2020GL087376

Williams, C. A., & Wallace, L. M. (2015). Effects of material property variations on slip estimates for subduction interface slow-slip events. *Geophysical Research Letters*, *42*(4), 1113–1121. https://doi.org/10.1002/2014GL062505

Zeng, Y., & Shen, Z. (2016). A fault-based model for crustal deformation, fault slip rates, and off-fault strain rate in California. *Bulletin of the Seismological Society of America*, *106*(2), 766–784. https://doi.org/10.1785/0120140250

Zeng, Y., & Shen, Z.-K. (2014). Fault network modeling of crustal deformation in California constrained using GPS and geologic observations. *Tectonophysics*, *612*, 1–17. https://doi.org/10.1016/j.tecto.2013.11.030

Zinke, R., Dolan, J. F., Rhodes, E. J., Van Dissen, R., McGuire, C. P., Hatem, A. E., et al. (2019). Multimillennial incremental slip rate variability of the Clarence fault at the tophouse road Site, Marlborough fault system, New Zealand. *Geophysical Research Letters*, *46*(2), 717–725. https://doi.org/10.1029/2018GL080688